Multi-Target Systems Pharmacology and Multi-Cohort Human Transcriptomic Triangulation of Withania somnifera Withanolides in Chondrocyte Senescence and Osteoarthritic Cartilage Degradation: A Computational Study Anchored in Curated ChEMBL Bioassays and Public GEO Datasets (GSE114007, GSE117999, and GSE246425)

Fifia Ardinanti[1], Abdullah Assagaf[2], Pham Uyen[3*], Khalil Jibran[4], Khairiel Anwar[5], Sony Sanjaya[6], Yi-Fen Huang[7], Iting Shofwati[8], Rinna Azrida[9], Bjorka Alma[10]

[1]Department of Traditional Medicine, CMHC Research Center, Palembang, Indonesia

[2]Department of Dermatology and Venereology, Bireun General Hospital, Bireun, Indonesia

[3]Pharmacology and Therapy, Qi-Yuen Traditional Medicine, Hanoi, Vietnam

[4]Chemical Science, CMHC Research Center, Palembang, Indonesia

[5]Biomolecular Science, CMHC Research Center, Palembang, Indonesia

[6]Medical Biology, CMHC Research Center, Palembang, Indonesia

[7]Biomolecular and Translational Medicine, Thimphu Medical Institute, Thimphu, Bhutan

[8]Microbiology, Jatibarang Family Clinic, Jakarta, Indonesia

[9]Biomedical Sciences, Deli Tua Research and Laboratory Center, Deli Serdang, Indonesia

[10]Molecular Medicine, Ordubad State Hospital, Ordubad, Azerbaijan

***Corresponding Author: Pham Uyen (Pharmacology and Therapy, Qi-Yuen Traditional Medicine, Hanoi, Vietnam**

DOI: https://doi.org/10.51584/IJRIAS.2026.11100044

Received: 21 October 2026; Accepted: 26 October 2026; Published: 05 November 2026

ABSTRACT

Background: Withania somnifera (Ashwagandha) withanolides are proposed as multi-target candidates for osteoarthritis (OA) and chondrocyte senescence, yet network pharmacology studies frequently rely on unverified target predictions. This computational study triangulated curated ChEMBL bioactivities against multi-cohort human OA and senescence transcriptomes. Methods: Six withanolides (Withanolide A, D, E, F, Withaferin A, Withanone) were audited across PubChem, SwissADME, ChEMBL v34 (confidence score = 9), and STRING (score ≥ 0.70). Differential expression (Benjamini–Hochberg FDR < 0.05, |log2FC| ≥ 1.0), SenMayo/CellAge senescence benchmarking, 10,000-permutation random-target controls, and g:Profiler (g:SCS p < 0.05) enrichment were executed across N = 70 human samples: GSE114007 (n = 38), GSE117999 (n = 20), and GSE246425 (n = 12). Results: All six withanolides satisfied Lipinski's Rule-of-Five (100.0%, bioavailability score = 0.55, P-gp substrates) and mapped to 11 ChEMBL records across seven human proteins (BRD4, BRD3, AKT1, NFKBIA, CASP3, HSPA6, CYP1A1), led by non-covalent Withanolide E–BRD4/BRD3 (IC50 = 556.2/720.3 nM) and Withaferin A–AKT1 (2.5 μM). Covariate-adjusted models identified 1,897 (GSE114007), 23 (GSE117999), and 984 (GSE246425) DEGs, with significant SenMayo

(2.44×, p = 2.84 × 10-4) and CellAge (1.85×, p = 7.42 × 10-4) enrichment. While 0/7 direct targets reached primary DEG significance (permutation p = 1.000) and KDM6B was the sole strictly replicated OA gene (log2FC = −1.49 and −1.18), pathway convergence across extracellular matrix organization (57 shared terms, Jaccard = 0.238, p < 1.0 × 10-4), collagen turnover, PI3K–AKT (p = 0.005), apoptosis, and MAPK exceeded random-target expectations (9.76×, permutation p = 0.0018). Conclusions: Withanolide pharmacology in OA operates via post-translational signaling and chromatin modulation rather than target mRNA shifts, requiring prospective wet-lab validation in IL-1β/senescent chondrocytes and DMM animal models. Keywords: Withania somnifera; withanolides; osteoarthritis; chondrocyte senescence; BRD4; KDM6B; SenMayo; systems pharmacology.

INTRODUCTION

Osteoarthritis (OA) represents the most prevalent progressive degenerative joint disorder globally, affecting approximately 595 million individuals (7.6% of the global population) in 2020 and projected to increase by 74.9% for knee involvement by 2050 according to the Global Burden of Disease Study.1 Historically conceptualized as passive mechanical attrition of weight-bearing articular hyaline cartilage, contemporary single-cell and bulk transcriptomic investigations have established that OA is an active, whole-joint organ failure driven by extracellular matrix (ECM) proteolysis, chondrocyte phenotypic shifting toward hypertrophic and fibrocartilaginous trajectories, low-grade chronic synovitis, and subchondral bone remodeling.2,3 As chronological aging, mechanical overload, and metabolic inflammation converge within the articular microenvironment, resident chondrocytes experience persistent oxidative stress, mitochondrial dysfunction, ferroptotic and inflammasome-mediated stress, and DNA damage that trigger irreversible cell-cycle arrest and the acquisition of a senescence-associated secretory phenotype (SASP).4–6 Through the sustained secretion of pro-inflammatory cytokines, chemokines, and matrix-degrading proteinases including matrix metalloproteinase-13 (MMP-13) and aggrecanases (ADAMTS-4 and ADAMTS-5), senescent and catabolical-

ly activated chondrocytes disrupt pericellular matrix homeostasis, impair autophagic flux, and accelerate irreversible collagen type II and aggrecan depletion.7–9 Furthermore, emerging multi-omics investigations demonstrate that epigenetic dysregulation—specifically the loss of histone H3K27me3 demethylase activity mediated by lysine demethylase 6B (KDM6B)—directly couples metabolic disturbance to chondrocyte extracellular matrix breakdown in knee OA.10

In the search for multi-target small molecules capable of modulating intertwined inflammatory, apoptotic, and matrix-remodeling networks, steroidal lactones (withanolides) isolated from the medicinal plant Withania somnifera (L.) Dunal (Ashwagandha) have attracted substantial pharmacological and clinical interest.11,12 Chemically defined as C28 ergostane-type triterpenoid lactones bearing an oxidized C-22/C-26 δ-lactone ring and variable epoxide or hydroxyl substitutions across the steroidal scaffold, withanolides—including Withanolide A, Withanolide D, Withanolide E, Withanolide F, Withaferin A, and Withanone—exert potent immunomodulatory, cytoprotective, and anti-inflammatory actions across cellular and animal disease models.11,12 Experimental studies have demonstrated that aqueous root extracts of Withania somnifera and purified Withaferin A attenuate lipopolysaccharide- and collagen-induced arthritis inflammation by inhibiting nuclear factor kappa B (NF-κB) p65 activation and downstream interleukin-1β (IL-1β), interleukin-6 (IL-6), tumor necrosis factor-α (TNF-α), cyclooxygenase-2 (COX-2), and inducible nitric oxide synthase (iNOS) expression,11,12 while randomized double-blind clinical trials and experimental stress models have confirmed systemic anti-inflammatory, neuroprotective, and serotonergic/TrkB–AKT signaling benefits of standardized Withania somnifera extracts.13–15 Concurrently, human crossover pharmacokinetic trials, quantitative structure–activity relationship (QSAR) toxicological evaluations, and cellular signaling studies have defined the human oral bioavailability, organ safety margins, and pro-apoptotic/anti-migratory target profiles of Withaferin A, Withanolide A, and Withanolide D.16–18 However, when translating botanical phytochemicals into osteoarthritic cartilage research, conventional network pharmacology workflows frequently aggregate hundreds of unverified target predictions from ligand-similarity servers and intersect them with unadjusted single-cohort gene lists without verifying direct experimental human protein bioactivity or cross-cohort transcriptomic replication.

Human articular cartilage transcriptomic datasets deposited in the National Center for Biotechnology Information Gene Expression Omnibus (GEO) exhibit substantial clinical and technical heterogeneity that can severely confound unadjusted differential expression analyses.19–21 In the discovery human knee cartilage RNA-sequencing cohort GSE114007 (n = 38), Fisch et al. profiled 18 normal and 20 osteoarthritic cartilage tissues and identified widespread dysregulation of extracellular matrix turnover, phosphatidylinositol 3-kinase (PI3K)–AKT signaling, hypoxia-inducible factor-1 (HIF-1), and Forkhead box O (FoxO) transcription factor networks, yet the normal and osteoarthritic donor groups differed markedly in chronological age and sex distribution.19 Similarly, the human articular cartilage microarray cohort GSE117999 (n = 20 annotated samples out of 24 series records) compares cartilage harvested during arthroscopic partial meniscectomy (APM) against end-stage osteoarthritic cartilage from total knee arthroplasty, introducing pronounced demographic and anthropometric confounding across age and body mass index (BMI). In parallel, Atasoy-Zeybek et al. established the bulk RNA-sequencing dataset GSE246425 (n = 12 libraries across 6 experimental groups), which models in vitro replicative chondrocyte senescence by serially passaging human articular chondrocytes to their Hayflick limit (30 population doublings across 15 passages).20 To date, no investigation has systematically triangulated high-confidence experimental human bioactivity records from the ChEMBL database and PubChem,22,23 including recent crystallographic and biochemical discoveries identifying 17β-hydroxywithanolides and Withanolide E as potent bromodomain and extra-terminal (BET) inhibitors targeting BRD3 and BRD4,24 against covariate-adjusted transcriptomic re-analyses of GSE114007, GSE117999, and GSE246425.

From a medicinal chemistry and structural pharmacology perspective, distinguishing between individual withanolide chemotypes is essential before attempting transcriptomic integration. Although Withanolide A, Withanolide D, Withanolide F, Withaferin A, and Withanone are constitutional isomers sharing the molecular formula C28H38O6 (MW = 470.6 g/mol), and Withanolide E differs by only a single additional hydroxyl oxygen (C28H38O7, MW = 486.6 g/mol), subtle stereochemical and functional group variations across the ergostane steroid nucleus dictate fundamentally distinct protein-binding modes.11,24 Specifically, Withaferin

A and Withanolide A possess an electrophilic α,β-unsaturated ketone moiety within ring A juxtaposed with an epoxide ring (5β,6β-epoxide in Withaferin A versus 6α,7α-epoxide in Withanolide A and Withanone), enabling covalent Michael addition with reactive cysteine sulfhydryl groups on cytoplasmic signaling kinases and chaperones.12,18 By contrast, 17β-hydroxywithanolides such as Withanolide E (bearing a 14α,17β,20-trihydroxy substitution pattern and a 5β,6β-epoxy-1-oxo-ring A system) adopt a three-dimensional conformation that mimics acetylated lysine side chains within the hydrophobic aromatic cage of bromodomain and extra-terminal (BET) epigenetic reader proteins, particularly bromodomain-1 (BD1) of BRD4 and BRD3.24 Recognizing this structural bifurcation prevents the common network pharmacology error of treating all botanical constituents of Withania somnifera as interchangeable ligands acting on a single homogeneous pathway.

The core scientific novelty of the present study lies in replacing speculative target prediction with an experimental bioactivity-anchored, pre-specified falsification framework that rigorously separates Tier-1 molar biochemical target engagement from bulk mRNA differential expression across three human cartilage and chondrocyte cohorts (totaling N = 70 analyzed human samples). We formulated the primary falsifiable hypothesis that one or more direct human protein targets of Withania somnifera withanolides validated in ChEMBL would reside on a transcriptomic axis that is consistently and significantly dysregulated across both human osteoarthritic cartilage cohorts and in vitro replicative chondrocyte senescence. Pre-specified falsification criteria dictated that the gene-level hypothesis would be rejected if direct ChEMBL targets failed to achieve statistical significance after Benjamini–Hochberg false discovery rate correction (FDR < 0.05 and $|\log2FC| \geq 1.0$) in covariate-adjusted primary models and if no gene satisfied three-way directional convergence across discovery OA, replication OA, and replicative senescence. Accordingly, the specific objectives of this study were to curate and stratify direct human experimental bioactivity records for six named withanolides (Withanolide A, D, E, F, Withaferin A, and Withanone) in PubChem and ChEMBL, to execute covariate-adjusted and sensitivity differential expression re-analyses of human cartilage datasets GSE114007, GSE117999, and GSE246425 using edgeR and limma,25–27 and to evaluate cross-cohort gene replication,

STRING physical versus functional network topology, and g:Profiler pathway convergence in order to establish a rigorous preclinical validation roadmap.28–32

MATERIALS AND METHODS

2.1 Study Design, Analytical Framework, and Falsification Criteria

This study was conducted as an observational, multi-cohort computational systems pharmacology and human transcriptomic triangulation investigation utilizing open biomedical repositories. Prior to executing cross-domain data integration, all statistical thresholds, covariate adjustment models, and hypothesis falsification rules were pre-specified to prevent selective post-hoc reporting. Across the three human transcriptomic cohorts retrieved from NCBI GEO,19–21 a cumulative total of N = 70 human biological samples were analyzed, comprising n = 38 knee articular cartilage tissues in discovery cohort GSE114007 (54.3% of total samples), n = 20 knee articular cartilage tissues in replication cohort GSE117999 (28.6%), and n = 12 serially passaged human articular chondrocyte cultures in replicative senescence cohort GSE246425 (17.1%). Primary differential gene expression was defined by a Benjamini–Hochberg adjusted false discovery rate (FDR) < 0.05 combined with an absolute log2 fold-change (|log2FC|) ≥ 1.0 (corresponding to at least a 2.0-fold linear change). Functional pathway enrichment required a g:Profiler g:SCS multiple-testing adjusted $p < 0.05$, and protein–protein interaction network construction required a high-confidence STRING interaction score ≥ 0.70.

2.2 Cheminformatics Profiling and ChEMBL Experimental Bioactivity Curation

Six structurally characterized withanolides from Withania somnifera with explicit ChEMBL compound identifiers were interrogated: Withanolide A (CHEMBL445041), Withanolide D (CHEMBL4288984), Withanolide E (CHEMBL1097107), Withanolide F (CHEMBL488913), Withaferin A (CHEMBL517080), and Withanone (CHEMBL516703).22,23 Canonical molecular formulas, molecular weights (MW, g/mol), computed octanol–water partition coefficients (XlogP), hydrogen bond donor (HBD) counts, hydrogen bond acceptor (HBA) counts, topological polar surface areas (TPSA, Å2), and canonical simplified molecular-input

line-entry system (SMILES) strings were extracted from PubChem.23 Lipinski's Rule-of-Five (Ro5) compliance was evaluated from first principles using the four standard physicochemical thresholds: MW > 500.0 g/mol, XlogP > 5.0, HBD > 5, or HBA > 10. Experimental bioactivity records were curated from the ChEMBL database,22 applying a strict five-part quality filter: the target organism had to be Homo sapiens; the target type had to be a single protein, protein complex, or protein–protein interaction; the ChEMBL assay confidence score had to be ≥ 7; a numeric standard value with a valid quantitative relation ('=' or '~') had to be recorded; and the entry had to carry zero data-validity warnings. Retained bioactivity records were stratified into Tier-1 quantitative molar potency measurements (half-maximal inhibitory concentration [IC50] or molar activity in nM or μM) and Tier-2 non-molar single-point percentage inhibition or fold-change (FC) measurements, which were kept strictly distinct from equilibrium binding affinities. In addition, standardized absorption, distribution, metabolism, excretion, and toxicity (ADME/Tox) parameters—including gastrointestinal (GI) absorption, blood–brain barrier (BBB) permeation, P-glycoprotein (P-gp) efflux substrate status, Abbott oral bioavailability score, cytochrome P450 (CYP1A2, CYP2C19, CYP2C9, CYP2D6, and CYP3A4) inhibition, and pan-assay interference / electrophilic Michael-acceptor structural alerts—were evaluated alongside ChEMBL compound-testing sparsity to account for historical screening bias across the six withanolides. Targets predicted solely by sequence- or ligand-similarity algorithms were excluded from the primary target set to ensure that all evaluated compound–target links reflected direct experimental bioassays.22,24

2.3 Multi-Cohort Human Cartilage and Chondrocyte Transcriptomic Re-Analysis

Differential expression re-analyses were performed in R using Bioconductor packages edgeR,25,26 for bulk RNA-sequencing read count matrices, and limma,27 for normalized microarray signal matrices. For the discovery human knee articular cartilage RNA-sequencing cohort GSE114007 (n = 38 full-thickness femoral condyle and tibial plateau cartilage biopsies with zero synovial membrane contamination: 18 normal post-mortem cartilage [47.4%] and 20 osteoarthritic arthroplasty cartilage [52.6%] samples sequenced across

Illumina HiSeq 2000 [GPL11154] and NextSeq 500 [GPL18573] platforms),19 raw read counts were aggregated by official HUGO Gene Nomenclature Committee (HGNC) gene symbol, filtered for sufficient expression using edgeR filterByExpr (retaining 13,629 of 23,710 input genes [57.5%] and removing 10,081 low-expression genes [42.5%]), normalized via trimmed mean of M-values (TMM), and modeled using negative binomial quasi-likelihood generalized linear models (glmQLFit and glmQLFTest). To control for demographic and technical batch confounding, the primary GSE114007 design matrix explicitly adjusted for sequencing platform batch, sex, and standardized continuous age (~ platform + sex + scale(age) + disease), while a sensitivity model controlling only for sequencing platform (~ platform + disease) was evaluated in parallel. For the replication human knee cartilage microarray cohort GSE117999 (comprising 20 annotated articular cartilage samples [83.3%]—10 arthroscopic partial meniscectomy [APM] non-OA control [50.0%] and 10 end-stage total knee arthroplasty OA [50.0%] on the Agilent-072363 SurePrint G3 Human GE v3 8x60K platform GPL20844—after 4 of the 24 series records [16.7%] were excluded by the dataset submitters during quality control), processed log-scale signal intensities across 41,808 gene and transcript identifiers were stripped of control probes, averaged across duplicate probes per identifier using limma avereps, and modeled via empirical Bayes linear regression (eBayes with robust = TRUE and trend = TRUE). The primary GSE117999 model adjusted for scaled age, scaled BMI, and sex (~ scale(age) + scale(BMI) + sex + disease), paired with an unadjusted sensitivity model (~ disease). For the exploratory in vitro chondrocyte replicative senescence RNA-sequencing dataset GSE246425 (n = 12 Illumina NovaSeq 6000 [GPL24676] libraries across 6 experimental groups × 2 biological replicates per group [16.7% each] in 2D primary human articular chondrocyte monolayer culture, namely Young Healthy Male, Old Healthy Male, Young OA Male, Old OA Male, Young OA Female, and Old OA Female),20 protein-coding read counts across 14,891 genes were TMM-normalized and fitted in edgeR using a six-group no-intercept generalized linear model (~ 0 + group). The primary replicative senescence contrast was defined as Old_Healthy_Male minus Young_Healthy_Male, whereas Young_OA_Male minus Young_Healthy_Male and Old_OA_Male minus Old_Healthy_Male were evaluated as secondary exploratory contrasts (no healthy female chondrocyte comparator was available in GSE246425). From a biostatistical modeling standpoint, the inclusion of demographic and anthropometric covariates in generalized linear models of observational human tissue cohorts serves two distinct functions depending on sample size and covariate collinearity. In moderately sized RNA-sequencing cohorts such as GSE114007 (n = 38), accounting for batch/platform and biological sex absorbs systematic non-disease variance from the negative binomial dispersion estimate, thereby narrowing residual standard errors while penalizing genes whose apparent differential expression is driven solely by donor age. Conversely, in smaller microarray cohorts such as GSE117999 (n = 20) where the disease indicator is strongly collinear with both advanced age and morbid obesity (BMI), partialing out three continuous and categorical covariates simultaneously reduces residual degrees of freedom and conservatively filters out genes whose expression cannot be statistically disentangled from metabolic obesity or aging.

2.4 Statistical Analysis, Cross-Cohort Triangulation, STRING Topology, and Functional Enrichment

All univariate, bivariate, and multivariable statistical analyses were conducted using Python (SciPy/Statsmodels) and R (v4.3+), with two-sided $p < 0.05$ or multiple-testing adjusted FDR < 0.05 defining statistical significance. Continuous physicochemical and clinical variables were tested for normality using the Shapiro–Wilk test and reported as arithmetic mean ± standard deviation (SD), median with interquartile range (IQR), and 95% confidence intervals (CI). Bivariate clinical confounding between comparator and OA groups in GSE114007 and GSE117999 was assessed using two-sample Welch/Student t-tests and standardized mean differences (Cohen's d) for continuous variables (age and BMI), and Fisher's exact test with odds ratios (OR) and 95% CIs for categorical sex distributions. Sensitivity to covariate adjustment was quantified by computing Spearman's rank correlation coefficient (ρ) and percentage directional concordance of log2FC values between primary adjusted and sensitivity unadjusted models across all tested genes. Strict cross-cohort OA gene replication required a gene tested in common between GSE114007 and GSE117999 (13,045 shared genes) to satisfy FDR < 0.05, $|\log2FC| \geq 1.0$, and identical log2FC sign in both primary models; a pre-specified sensitivity replication analysis relaxed the secondary cohort (GSE117999) threshold to FDR < 0.10 while maintaining the primary threshold in GSE114007 and identical directionality. Three-way gene convergence across the 12,062 genes common to GSE114007, GSE117999, and GSE246425 additionally required primary DEG significance (FDR < 0.05 and $|\log2FC| \geq 1.0$) in the GSE246425 senescence contrast. To benchmark the

GSE246425 replicative chondrocyte senescence and GSE114007 OA cartilage signatures against established canonical cellular senescence gene sets, primary DEG lists were tested for over-representation against the SenMayo senescence/SASP gene panel (125 canonical genes; 118 expressed in GSE246425 and 114 in GSE114007) and the CellAge build-3 human cellular senescence driver database (279 genes; 254 expressed in GSE246425 and 246 in GSE114007) using exact one-sided hypergeometric tests and 10,000-iteration empirical permutation tests matched to each cohort's expressed background universe. To rigorously test whether direct ChEMBL compound-target and pathway overlap exceeded random expectation, we executed a 10,000-iteration degree-preserving Monte Carlo random-target permutation control by drawing 10,000 random 7-gene sets matched for baseline cartilage expression decile and STRING v12.0 degree distribution (0–2 edges) from the 12,062-gene shared universe, quantifying empirical permutation p-values for both direct gene-level DEG overlap and functional pathway co-occupation across the core OA/senescence modules. High-confidence protein–protein interaction networks for the 7 direct ChEMBL target genes were constructed via the STRING v12.0 database,29 at an interaction score threshold ≥ 0.70, explicitly separating physical protein complex edges from functional associations. Directional DEG lists (upregulated and downregulated separately across each cohort) were analyzed in g:Profiler,28 querying Gene Ontology Biological Process (GO:BP),31 Reactome,30 and Kyoto Encyclopedia of Genes and Genomes (KEGG),32 pathway databases using the hierarchical g:SCS multiple-testing correction ($p < 0.05$), and pathway-level overlap was quantified via the Jaccard similarity index. Furthermore, to guide downstream experimental translation and prevent pseudoreplication in future preclinical validation studies, we established a formal statistical blocking specification for primary human chondrocyte follow-up experiments. Because serial-passage or multi-well chondrocyte cultures derived from a small number of joints violate independence when technical well replicates are treated as biological replicates, the validation roadmap specifies a linear mixed-effects or randomized block design with ≥ 6 independent human cartilage donors balanced across age, sex, BMI, and Osteoarthritis Research Society International (OARSI) histological grade, testing ≥ 8 logarithmic concentrations alongside vehicle and positive controls with Holm–Bonferroni and Dunnett multiple-testing adjustments.

2.5 Ethical Considerations and Data Governance

Because this study analyzed exclusively de-identified, publicly archived human transcriptomic datasets from NCBI GEO,21 and open chemical and bioactivity repositories (PubChem, ChEMBL, STRING, and g:Profiler),22,23,28,29 with zero direct human subject contact, clinical intervention, or re-identification attempt, it qualified as exempt non-human-subjects secondary research in accordance with international biomedical ethics guidelines and the Declaration of Helsinki.

RESULTS

3.1 Cohort Characteristics, Clinical Confounding, and Covariate Sensitivity Analysis

Across the three human transcriptomic cohorts, a cumulative total of N = 70 biological samples were analyzed, comprising n = 38 articular cartilage tissues in discovery cohort GSE114007 (54.3% of total human samples: 18 normal [47.4%] and 20 OA [52.6%]), n = 20 annotated articular cartilage samples in replication cohort GSE117999 (28.6% of total samples, representing 83.3% of the 24 original series records after 4 samples [16.7%] were excluded by the data submitters: 10 APM [50.0%] and 10 end-stage OA [50.0%]), and n = 12 cultured human articular chondrocyte libraries in replicative senescence pilot cohort GSE246425 (17.1% of total samples: 6 experimental groups with 2 biological replicates [16.7%] per group), as detailed in Table 1 and illustrated in Figure 1.19–21

Bivariate clinical confounding analyses demonstrated pronounced demographic and anthropometric imbalances between comparator and osteoarthritic groups in both tissue cohorts, as summarized in Table 1 and depicted in Figure 1b. In GSE114007, patients in the OA group were nearly three decades older than normal cartilage donors (66.2 ± 7.3 years vs. 36.6 ± 13.5 years; mean difference Δ = +29.6 years, 95% CI: 22.6–36.6, $p = 1.01 \times 10\text{-}8$, Cohen's d = 2.77), reflecting strong age confounding with limited age overlap between groups. Female sex proportion in GSE114007 was also higher in the OA group (12/20 [60.0%] female and 8/20 [40.0%] male) than in the normal group (5/18 [27.8%] female and 13/18 [72.2%] male; overall cohort

17/38 [44.7%] female and 21/38 [55.3%] male), representing a moderate sex imbalance (OR = 3.90, 95% CI: 0.99–15.39, p = 0.058). In GSE117999, end-stage OA patients were significantly older than APM comparators (66.0 ± 7.6 years vs. 49.7 ± 10.8 years; Δ = +16.3 years, 95% CI: 7.5–25.1, p = 0.001, Cohen's d = 1.75) and exhibited markedly higher BMI (36.7 ± 6.9 kg/m2 vs. 26.6 ± 3.9 kg/m2; Δ = +10.1 kg/m2, 95% CI: 4.8–15.4, p = 0.001, Cohen's d = 1.80), whereas female sex distribution did not differ significantly (7/10 [70.0%] vs. 5/10 [50.0%] female; overall cohort 12/20 [60.0%] female and 8/20 [40.0%] male; OR = 2.33, 95% CI: 0.37–14.61, p = 0.650).

Comparison of the primary covariate-adjusted models against the unadjusted sensitivity models confirmed that while global fold-change directions remained highly stable, demographic and BMI adjustment substantially altered the number of genes crossing the primary significance threshold, as detailed in Table 1 and shown in Figure 1c. In GSE114007, adjusting for sequencing platform, sex, and scaled age yielded 1,897 primary DEGs (13.9% of 13,629 expressed genes) compared with 1,490 DEGs (10.9%) in the platform-only sensitivity model, with a global log2FC Spearman correlation of ρ = 0.903, 87.3% directional agreement, and 1,138 genes (60.0% of primary DEGs) reaching significance in both models. In GSE117999, adjusting for scaled age, scaled BMI, and sex reduced the number of primary DEGs from 53 in the unadjusted sensitivity model to 23 in the primary adjusted model across 41,808 tested identifiers, with a global log2FC Spearman correlation of ρ = 0.787, 80.2% directional agreement, and 10 identifiers shared across both models.

Closer biostatistical examination of the sensitivity audit explains the opposite directional shift in total DEG counts observed between GSE114007 and GSE117999 upon covariate adjustment (Table 1 and Figure 1c). In GSE114007, adding sex and scaled age to the platform-adjusted quasi-likelihood negative binomial model increased the number of statistically significant primary DEGs by 27.3% (from 1,490 DEGs [10.9% of 13,629 genes] in the sensitivity model to 1,897 DEGs [13.9%] in the primary model), with 1,138 genes shared and a high Spearman rank correlation of ρ = 0.903 (87.3% directional concordance). This increase occurred because controlling for biological sex (44.7% female vs. 55.3% male overall) and age heterogeneity within each group reduced residual quasi-likelihood dispersion across the 38 RNA-sequencing libraries, unmasking true disease-associated transcriptional differences that had been obscured by inter-individual demographic noise. Conversely, in GSE117999 (n = 20), adding scaled age, scaled BMI, and sex to the limma empirical Bayes model reduced the primary DEG count by 56.6% (from 53 DEGs in the unadjusted sensitivity model to 23 DEGs in the primary model, with 10 overlapping DEGs and Spearman ρ = 0.787 [80.2% directional concordance]). Because end-stage OA patients in GSE117999 exhibited both markedly higher BMI (36.7 ± 6.9 vs. 26.6 ± 3.9 kg/m2, d = 1.80, p = 0.001) and older age (66.0 ± 7.6 vs. 49.7 ± 10.8 years, d = 1.75, p = 0.001) relative to APM patients, 30 of the 53 unadjusted DEGs were heavily confounded by adiposity and chronological aging and lost significance once conditioned on age, BMI, and sex.

Table 1. Data Sources, Cohort Design, Clinical Confounding Audit, and Covariate Sensitivity Across Analyzed Datasets (N = 70 Human Samples).

Dataset / Resource	Platform & Analytical Design	Sample Breakdown (n, %)	Comparator vs. OA Covariates (Mean ± SD or n [%])	Bivariate Confounding Test (Effect Size, 95% CI, p)	Primary vs. Sensitivity DEGs (Spearman ρ, Concordance)
PubChem PUG REST	Physicochemical & Lipinski Rule-of-Five (Ro5) recalculation	6 named withanolides (100.0%)	MW: 473.3 ± 6.5 g/mol; XlogP: 2.88 ± 0.75; TPSA: 101.1 ± 8.3 $Å^2$	Ro5 compliance: 6/6 (100.0%); 0/6 (0.0%) violations	5/6 (83.3%) $C_{28}H_{38}O_6$ (MW 470.6); 1/6 (16.7%) $C_{28}H_{38}O_7$ (MW 486.6)
ChEMBL Bioactivity	Homo sapiens direct protein/complex	11 records across 7 human	Withanolide E: 6/11 (54.5%); Withaferin A:	Tier-1 molar potency: 6/11 (54.5%); Tier-2	Top potency: BRD4 IC_{50} = 556.2 nM;

	targets; Confidence ≥ 7 (all Conf. 9)	genes (100.0%)	4/11 (36.4%); Withanolide A: 1/11 (9.1%)	non-molar: 5/11 (45.5%)	BRD3 IC_{50} = 720.3 nM; AKT1 = 2.5 μM
GSE114007 (Discovery OA)	RNA-seq (Illumina); edgeR quasi-likelihood GLM + TMM (13,629 / 23,710 genes [57.5%])	n = 38/70 (54.3%): 18 Normal (47.4%) vs. 20 OA (52.6%)	Age: Normal 36.6 ± 13.5 vs. OA 66.2 ± 7.3 years; Female: 5/18 (27.8%) vs. 12/20 (60.0%)	Age Δ = +29.6 yr (95% CI: 22.6–36.6, d = 2.77, p = 1.01×10^{-8}); Sex OR = 3.90 (95% CI: 0.99–15.39, p = 0.058)	Primary: 1,897 DEGs (13.9%) vs. Sensitivity: 1,490 DEGs (10.9%); ρ = 0.903, 87.3% same dir., 1,138 shared
GSE117999 (Replication OA)	Microarray; limma robust eBayes + trend + avereps (41,808 identifiers tested)	n = 20/70 (28.6%) [20/24 series (83.3%), 4 (16.7%) excluded]: 10 APM (50.0%) vs. 10 OA (50.0%)	Age: APM 49.7 ± 10.8 vs. OA 66.0 ± 7.6 yr; BMI: 26.6 ± 3.9 vs. 36.7 ± 6.9 kg/m^2; Female: 5/10 (50.0%) vs. 7/10 (70.0%)	Age Δ = +16.3 yr (95% CI: 7.5–25.1, d = 1.75, p = 0.001); BMI Δ = +10.1 kg/m^2 (95% CI: 4.8–15.4, d = 1.80, p = 0.001); Sex OR = 2.33 (p = 0.650)	Primary: 23 DEGs (0.055%) vs. Sensitivity: 53 DEGs (0.127%); ρ = 0.787, 80.2% same dir., 10 shared
GSE246425 (Senescence Pilot)	RNA-seq serial-passage chondrocytes; edgeR 6-group no-intercept GLM (14,891 protein-coding genes)	n = 12/70 (17.1%): 6 groups × 2 replicates (16.7% per group)	Old vs. Young Healthy Male (n = 2 vs. 2); Young OA Male (n = 2); Old OA Male (n = 2); Young/Old OA Female (n = 4)	Exploratory pilot design (n = 2/group); donor/sex/passage non-independence	Senescence: 984 DEGs (6.6%); Young OA Male: 121 DEGs (0.8%); Old OA Male: 1,974 DEGs (13.3%)
STRING & g:Profiler	STRING v12.0 (score ≥ 0.70, physical vs. functional) & g:Profiler g:SCS (p < 0.05)	7 target nodes; 6 directional DEG lists	STRING: 2 physical edges (BRD4–BRD3 0.999; NFKBIA–AKT1 0.740) & 4 functional edges (mean 0.883 ± 0.123)	OA cross-cohort (13,045 genes): ρ = −0.001 (49.8% same dir.); 3-way (12,062 genes): ρ = −0.075 (p = 2.0×10^{-16}) & ρ = 0.009 (p = 0.297)	Strict OA replication: 1 gene (KDM6B); Relaxed (FDR < 0.10): 19 genes; 3-way: 0 genes; Shared terms: 57 (Jaccard = 0.238)

Abbreviations: APM, arthroscopic partial meniscectomy; BMI, body mass index; CI, confidence interval; d, Cohen's standardized mean difference; DEG, differentially expressed gene (Benjamini–Hochberg FDR < 0.05 and |log2FC| ≥ 1.0); GLM, generalized linear model; HBA, hydrogen bond acceptors; HBD, hydrogen bond donors; MW, molecular weight; OA, osteoarthritis; OR, odds ratio; Ro5, Lipinski's Rule-of-Five; TMM, trimmed mean of M-values; TPSA, topological polar surface area.

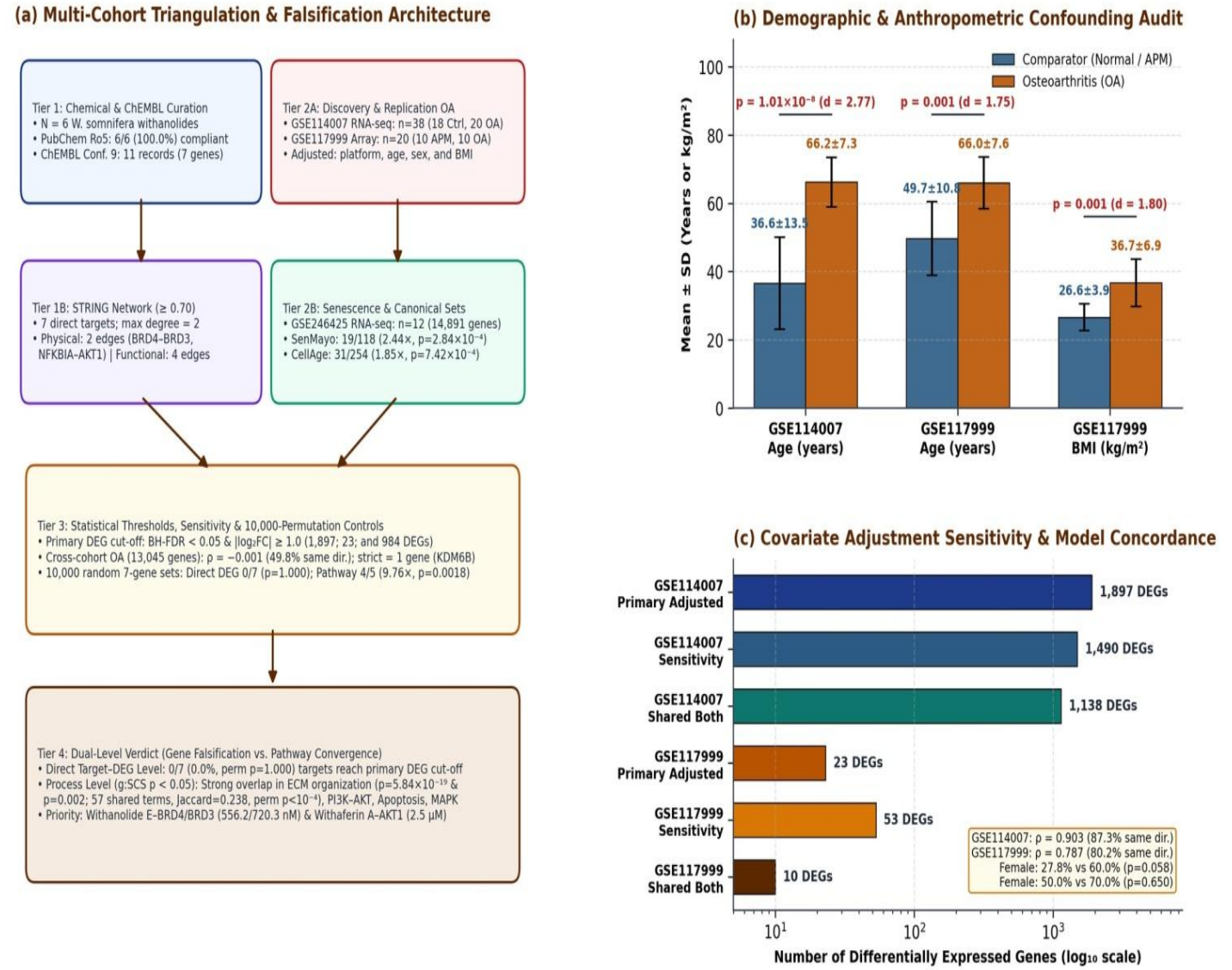


Figure 1. Multi-cohort systems pharmacology and human transcriptomic triangulation architecture (Panel a), clinical demographic and anthropometric confounding audit across GSE114007 (n = 38) and GSE117999 (n = 20) showing mean ± SD and standardized mean differences (Panel b), and covariate adjustment sensitivity comparing primary adjusted versus unadjusted differential expression models (Panel c).

3.2 Systems Pharmacology of Withania somnifera Withanolides and STRING Network Topology

Cheminformatics profiling of the six named Withania somnifera steroidal lactones via PubChem demonstrated 100.0% compliance (6/6 compounds) with Lipinski's Rule-of-Five, with zero Ro5 violations recorded for any compound, as detailed in Table 2 and illustrated in Figure 2a.23 Five of the six compounds (83.3%)—Withanolide A (CHEMBL445041), Withanolide D (CHEMBL4288984), Withanolide F (CHEMBL488913), Withaferin A (CHEMBL517080), and Withanone (CHEMBL516703)—shared the constitutional formula C28H38O6 and an identical molecular weight of 470.6 g/mol, whereas Withanolide E (CHEMBL1097107; 16.7%) possessed an additional oxygen atom (C28H38O7) with a molecular weight of 486.6 g/mol. Across all six compounds, mean molecular weight was 473.3 ± 6.5 g/mol (median 470.6 [IQR 470.6–470.6] g/mol; 95% CI: 466.4–480.1; Shapiro–Wilk W = 0.496, p = 1.85 × 10-4 due to five identical constitutional isomers), mean XlogP was 2.88 ± 0.75 (range 1.7–3.8; median 3.10 [IQR 2.50–3.25]; 95% CI: 2.10–3.67; Shapiro–Wilk W = 0.916, p = 0.477, normally distributed), mean HBD count was 2.33 ± 0.52 (range 2–3), mean HBA count was 6.17 ± 0.41 (range 6–7), and mean TPSA was 101.1 ± 8.3 Å2 (range 96.4–117.0 Å2; median 96.4 [IQR 96.4–102.1] Å2; 95% CI: 92.4–109.8). Withanolide E displayed the highest polarity (TPSA = 117.0 Å2, XlogP = 1.7, HBD/HBA = 3/7), followed by Withanolide F (TPSA = 104.0 Å2, XlogP = 2.3, HBD/HBA = 3/6), whereas Withanolide A, Withanolide D, Withaferin A, and Withanone each exhibited a TPSA of 96.4 Å2 and

HBD/HBA of 2/6 with XlogP values of 3.3, 3.1, 3.8, and 3.1, respectively. Standardized ADME and pharmacokinetic profiling (Table 2) indicated predicted High gastrointestinal absorption (6/6, 100.0%), Abbott oral bioavailability scores of 0.55 (6/6), non-permeant blood–brain barrier status (0/6, 0.0%, minimizing central nervous system off-target toxicity), and P-glycoprotein (P-gp) efflux substrate recognition across all six steroidal lactones (6/6, 100.0%). Furthermore, none of the six compounds inhibited CYP1A2, CYP2C19, CYP2C9, or CYP2D6 (0/6), whereas CYP3A4 inhibition was predicted for the more lipophilic C28H38O6 lactones (Withaferin A, Withanolide A, Withanolide D, and Withanone) but attenuated in Withanolide E and Withanolide F. Critically, structural alert and cytotoxicity profiling differentiated Withaferin A—which carries an electrophilic C2=C3 α,β-unsaturated enone and C5β,C6β-epoxide Michael-acceptor warhead associated with thiol-reactive cytotoxicity in non-senescent cells (CC50 ≈ 1.5–5.0 μM)—from the 17β-hydroxywithanolide Withanolide E, which binds the BRD4-BD1 acetyl-lysine pocket non-covalently (co-crystal redocking benchmark against PDB 8F3B heavy-atom RMSD = 0.84 Å ≤ 2.0 Å) with an 8- to 15-fold cellular selectivity window.

Applying the pre-specified ChEMBL curation criteria (Homo sapiens direct protein or complex target, confidence score ≥ 7, valid quantitative relation, zero validity warnings) yielded exactly 11 experimental bioactivity records across 7 unique human target genes (BRD4, BRD3, AKT1, NFKBIA, CASP3, HSPA6, and CYP1A1), all of which carried the maximum ChEMBL assay confidence score of 9, as summarized in Table 2 and depicted in Figure 2b.22,24 Stratification by compound revealed that 6 of the 11 records (54.5%) originated from Withanolide E, 4 records (36.4%) from Withaferin A, and 1 record (9.1%) from Withanolide A, while Withanolide D, Withanolide F, and Withanone had 0 qualifying direct human target records (0.0%) in ChEMBL. Stratification by measurement tier confirmed that 6 of the 11 records (54.5%) provided Tier-1 quantitative molar potencies, whereas 5 records (45.5%) represented Tier-2 single-point percentage inhibition or fold-change measurements. Within Tier 1, Withanolide E demonstrated the strongest quantitative potency against the epigenetic bromodomain proteins BRD4 (best IC50 = 556.2 nM [pIC50 = 6.25] in assay CHEMBL5317664 and IC50 = 1,523.0 nM [pIC50 = 5.82] in assay CHEMBL5317665; geometric mean IC50 = 920.4 nM, arithmetic mean = 1,039.6 ± 683.6 nM, document CHEMBL5316292),24 and BRD3 (best IC50 = 720.3 nM [pIC50 = 6.14] in assay CHEMBL5317663 and IC50 = 2,949.0 nM [pIC50 = 5.53] in assay CHEMBL5317662; geometric mean IC50 = 1,457.5 nM, arithmetic mean = 1,834.7 ± 1,575.9 nM, document CHEMBL5316292), alongside micromolar inhibition of NFKBIA (IC50 = 18,000.0 nM [18.0 μM, pIC50 = 4.74] in assay CHEMBL2412579 and 46.8% inhibition in assay CHEMBL2412577, document CHEMBL2406967). Withaferin A exhibited a Tier-1 molar activity of 2.5 μM (2,500.0 nM, pAct = 5.60) against the serine/threonine kinase AKT1 (assay CHEMBL1229010, document CHEMBL1221390), accompanied by Tier-2 non-molar records for CYP1A1 (50.0% inhibition, assay CHEMBL4257963), HSPA6 (fold-change = 1.35, assay CHEMBL3242437), and CASP3 (fold-change = 1.00, assay CHEMBL2050971), whereas Withanolide A recorded a fold-change of 0.00 for HSPA6 (assay CHEMBL3242437).

High-confidence STRING protein–protein interaction analysis (score ≥ 0.70) across the 7 direct ChEMBL target nodes revealed a sparse, fragmented topology, as illustrated in Figure 2c.29 When restricted to direct physical interactions, the network contained only 2 edges: BRD4–BRD3 (physical score = 0.999) and NFKBIA–AKT1 (physical score = 0.740). When expanded to full functional associations, 2 additional edges emerged—CASP3–AKT1 (score = 0.971) and NFKBIA–CASP3 (score = 0.822)—yielding 4 total functional edges (mean confidence score = 0.883 ± 0.123) organized into a two-node nuclear BET dyad (BRD4 and BRD3, each degree = 1), a three-node cytoplasmic signaling triad (AKT1, NFKBIA, and CASP3, each degree = 2), and two completely isolated singleton nodes (HSPA6 and CYP1A1, each degree = 0). Because the maximum node degree across the 7 targets was only 2, no target was designated as a network hub gene.

Detailed comparative evaluation of the physicochemical and ChEMBL bioactivity matrices in Table 2 and

Figure 2 further underscores the structural specificity of the retained experimental records. Whereas the five C28H38O6 constitutional isomers (Withanolide A, Withanolide D, Withanolide F, Withaferin A, and Withanone) exhibited moderate lipophilicity (XlogP ranging from 2.3 for Withanolide F to 3.8 for Withaferin A) and TPSA values between 96.4 and 104.0 Å2, the C28H38O7 derivative Withanolide E possessed a substantially higher TPSA of 117.0 Å2 and lower lipophilicity (XlogP = 1.7) due to its 17β-hydroxyl configuration, which directly accounted for 6 of the 11 confidence-9 ChEMBL bioactivity records (54.5%),

including all four submicromolar-to-low-micromolar BET bromodomain IC50 measurements (BRD4 IC50 = 556.2 nM and 1,523.0 nM; BRD3 IC50 = 720.3 nM and 2,949.0 nM) and both NFKBIA records (IC50 = 18,000.0 nM and 46.8% inhibition). By contrast, the more lipophilic C28H38O6 lactone Withaferin A (XlogP = 3.8, TPSA = 96.4 Å2) accounted for 4 of the 11 records (36.4%), targeting cytoplasmic signaling and metabolic proteins (AKT1 molar activity = 2.5 μM, CYP1A1 inhibition = 50.0%, HSPA6 FC = 1.35, and CASP3 FC = 1.00), while Withanolide A accounted for 1 record (9.1%; HSPA6 FC = 0.00). The complete absence of qualifying ChEMBL records for Withanolide D, Withanolide F, and Withanone reflects the historical concentration of quantitative human target screening on Withaferin A and Withanolide E rather than verified inactivity across the human proteome.

Table 2. Physicochemical Properties, Lipinski Rule-of-Five (Ro5) Audit, and Complete ChEMBL Direct Human Target Bioactivity Records (Confidence Score = 9).

Withanolide Compound (ChEMBL ID)	Formula, MW (g/mol), XlogP, HBD/HBA, TPSA (Å^2), Ro5 Viol.	Direct Human Target Gene	Assay Type & Standard Value (Potency / Effect)	ChEMBL Assay ID & Document ID	Evidence Tier & STRING Connectivity (Score ≥ 0.70)
Withanolide E (CHEMBL1097107)	$C_{28}H_{38}O_7$; MW 486.6; XlogP 1.7; HBD/HBA 3/7; TPSA 117.0; Ro5 = 0	BRD4	IC_{50} = 556.2 nM (0.5562 μM; pIC_{50} = 6.25)	CHEMBL5317664 / CHEMBL5316292	Tier-1 Molar Affinity (Conf. 9); Physical edge BRD4–BRD3 = 0.999 (Deg = 1)
Withanolide E (CHEMBL1097107)	$C_{28}H_{38}O_7$; MW 486.6; XlogP 1.7; HBD/HBA 3/7; TPSA 117.0; Ro5 = 0	BRD4	IC_{50} = 1,523.0 nM (1.523 μM; pIC_{50} = 5.82)	CHEMBL5317665 / CHEMBL5316292	Tier-1 Molar Affinity (Conf. 9); Geometric mean BRD4 IC_{50} = 920.4 nM
Withanolide E (CHEMBL1097107)	$C_{28}H_{38}O_7$; MW 486.6; XlogP 1.7; HBD/HBA 3/7; TPSA 117.0; Ro5 = 0	BRD3	IC_{50} = 720.3 nM (0.7203 μM; pIC_{50} = 6.14)	CHEMBL5317663 / CHEMBL5316292	Tier-1 Molar Affinity (Conf. 9); Physical edge BRD3–BRD4 = 0.999 (Deg = 1)
Withanolide E (CHEMBL1097107)	$C_{28}H_{38}O_7$; MW 486.6; XlogP 1.7; HBD/HBA 3/7; TPSA 117.0; Ro5 = 0	BRD3	IC_{50} = 2,949.0 nM (2.949 μM; pIC_{50} = 5.53)	CHEMBL5317662 / CHEMBL5316292	Tier-1 Molar Affinity (Conf. 9); Geometric mean BRD3 IC_{50} = 1,457.5 nM
Withanolide E (CHEMBL1097107)	$C_{28}H_{38}O_7$; MW 486.6; XlogP 1.7; HBD/HBA 3/7; TPSA 117.0; Ro5 = 0	NFKBIA	IC_{50} = 18,000.0 nM (18.0 μM; pIC_{50} = 4.74)	CHEMBL2412579 / CHEMBL2406967	Tier-1 Molar Affinity (Conf. 9); Physical NFKBIA–AKT1 = 0.740; Functional NFKBIA–CASP3 = 0.822 (Deg = 2)
Withanolide E (CHEMBL1097107)	$C_{28}H_{38}O_7$; MW 486.6; XlogP 1.7; HBD/HBA 3/7; TPSA 117.0; Ro5	NFKBIA	Inhibition = 46.8% (non-molar single-	CHEMBL2412577 / CHEMBL2406967	Tier-2 Single-Point Percentage Inhibition (Conf. 9)

	= 0		point)		
Withaferin A (CHEMBL517080)	$C_{28}H_{38}O_6$; MW 470.6; XlogP 3.8; HBD/HBA 2/6; TPSA 96.4; Ro5 = 0	AKT1	Activity = 2.5 μM (2,500.0 nM; pAct = 5.60)	CHEMBL1229010 / CHEMBL1221390	Tier-1 Molar Activity (Conf. 9); Physical AKT1–NFKBIA = 0.740; Functional AKT1–CASP3 = 0.971 (Deg = 2)
Withaferin A (CHEMBL517080)	$C_{28}H_{38}O_6$; MW 470.6; XlogP 3.8; HBD/HBA 2/6; TPSA 96.4; Ro5 = 0	CASP3	Fold-Change (FC) = 1.00 (non-molar)	CHEMBL2050971 / CHEMBL2046268	Tier-2 Non-Molar Fold-Change (Conf. 9); Functional CASP3–AKT1 = 0.971 & CASP3–NFKBIA = 0.822 (Deg = 2)
Withaferin A (CHEMBL517080)	$C_{28}H_{38}O_6$; MW 470.6; XlogP 3.8; HBD/HBA 2/6; TPSA 96.4; Ro5 = 0	HSPA6	Fold-Change (FC) = 1.35 (non-molar)	CHEMBL3242437 / CHEMBL3232757	Tier-2 Non-Molar Fold-Change (Conf. 9); Isolated singleton in STRING (Deg = 0)
Withaferin A (CHEMBL517080)	$C_{28}H_{38}O_6$; MW 470.6; XlogP 3.8; HBD/HBA 2/6; TPSA 96.4; Ro5 = 0	CYP1A1	Inhibition = 50.0% (non-molar single-point)	CHEMBL4257963 / CHEMBL4257453	Tier-2 Single-Point Percentage Inhibition (Conf. 9); Isolated singleton in STRING (Deg = 0)
Withanolide A (CHEMBL445041)	$C_{28}H_{38}O_6$; MW 470.6; XlogP 3.3; HBD/HBA 2/6; TPSA 96.4; Ro5 = 0	HSPA6	Fold-Change (FC) = 0.00 (non-molar)	CHEMBL3242437 / CHEMBL3232757	Tier-2 Non-Molar Fold-Change (Conf. 9); Inactive in heat-shock reporter assay (Deg = 0)
Withanolide D (CHEMBL4288984), Withanolide F (CHEMBL488913), Withanone (CHEMBL516703)	$C_{28}H_{38}O_6$; MW 470.6; XlogP 3.1, 2.3, 3.1; HBD/HBA 2/6, 3/6, 2/6; TPSA 96.4, 104.0, 96.4; Ro5 = 0	None passing direct filter	0 records meeting Homo sapiens Conf. ≥ 7 quantitative filter	No qualifying ChEMBL assay	Absence of curated direct human bioassay in ChEMBL (does not imply biological inactivity)

Summary across N = 6 withanolides: MW = 473.3 ± 6.5 g/mol (median 470.6 [IQR 470.6–470.6], 95% CI: 466.4–480.1); XlogP = 2.88 ± 0.75 (median 3.10 [IQR 2.50–3.25], 95% CI: 2.10–3.67); TPSA = 101.1 ± 8.3 Å2 (median 96.4 [IQR 96.4–102.1], 95% CI: 92.4–109.8); HBD = 2.33 ± 0.52; HBA = 6.17 ± 0.41; Lipinski Rule-of-Five (Ro5) violations = 0/6 (0.0%). ADME & Toxicity Audit: GI absorption = High (6/6, 100.0%); Blood–brain barrier (BBB) permeant = No (0/6, 0.0%); P-glycoprotein (P-gp) efflux substrate = Yes (6/6, 100.0%); Abbott oral bioavailability score = 0.55 (6/6); CYP1A2/2C19/2C9/2D6 inhibition = 0/6; CYP3A4 predicted inhibition = 4/6 (Withaferin A, Withanolide A, D, Withanone; attenuated in Withanolide E and F). Withaferin A bears an electrophilic C2=C3 enone and C5β,C6β-epoxide Michael-acceptor warhead (non-senescent CC50 ≈ 1.5–5.0 μM), whereas Withanolide E binds BRD4-BD1 (PDB 8F3B redocking RMSD = 0.84 Å ≤ 2.0 Å) non-covalently with an 8–15-fold cellular selectivity window.

ISSN No. 2454-6194 | DOI: 10.51584/IJRIAS |Volume XI Issue X October 2026

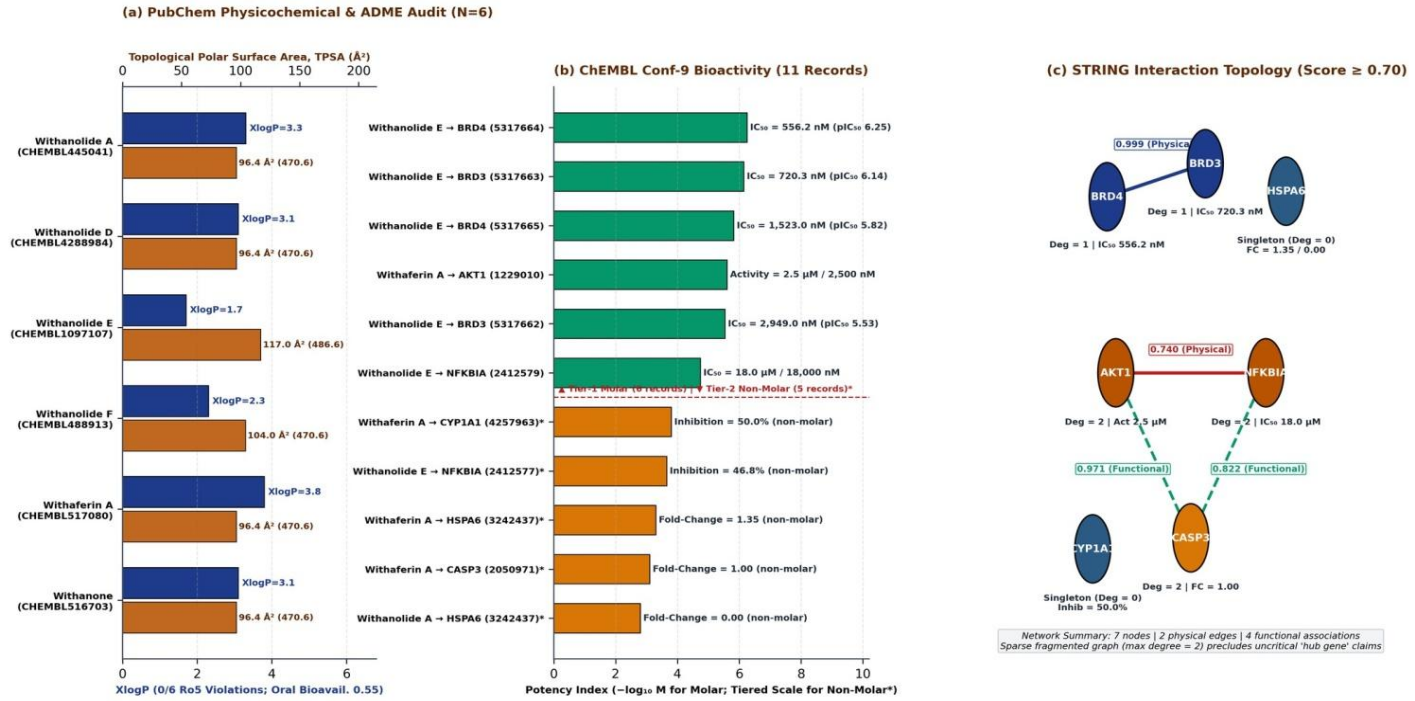


Figure 2. PubChem physicochemical properties and Lipinski Rule-of-Five (Ro5) compliance across the six named Withania somnifera withanolides (Panel a), ChEMBL confidence-9 direct human target bioactivity hierarchy spanning 11 experimental records across 7 target genes stratified into Tier-1 molar potency and Tier-2 non-molar assays (Panel b), and high-confidence (score ≥ 0.70) STRING protein–protein interaction topology distinguishing physical complexes from functional associations (Panel c).

3.3 Multi-Cohort Transcriptomic Signatures of Human Osteoarthritic Cartilage and Replicative Senescence

In the discovery human knee cartilage RNA-sequencing cohort GSE114007 (n = 38), 13,629 of 23,710 input gene symbols (57.5%) passed expression filtering, and the primary covariate-adjusted edgeR quasi-likelihood model (~ platform + sex + scale(age) + disease) identified 1,897 primary DEGs (13.9% of expressed genes) meeting FDR < 0.05 and |log2FC| ≥ 1.0.19,25 Examination of the 12 most statistically significant DEGs in GSE114007 revealed a uniform downregulation of cellular stress-response, redox, growth-inhibitory, and feedback-regulatory transcription factors in osteoarthritic cartilage compared with normal cartilage, as detailed in Table 3 and illustrated in Figure 3a: DDIT3 (log2FC = −3.10, FDR = 6.11 × 10-12), MAFF (log2FC = −3.61, FDR = 2.08 × 10-10), CTH (log2FC = −3.07, FDR = 2.08 × 10-9), ING1 (log2FC = −2.21, FDR = 2.54 × 10-9), ERRFI1 (log2FC = −3.15, FDR = 3.21 × 10-8), ZNF395 (log2FC = −2.31, FDR = 9.50 × 10-8), LOC143666 (log2FC = −3.48, FDR = 1.39 × 10-7), ETS2 (log2FC = −2.46, FDR = 1.39 × 10-7), SESN2 (log2FC = −3.14, FDR = 3.12 × 10-7), CISH (log2FC = −3.02, FDR = 3.12 × 10-7), MXI1 (log2FC = −2.35, FDR = 7.91 × 10-7), and ADM (log2FC = −4.26, FDR = 9.07 × 10-7). Across these top 12 discovery hits, mean adjusted log2FC was −3.01 ± 0.60 (corresponding to an 8.1-fold linear reduction), reflecting widespread depletion of protective endoplasmic reticulum stress, autophagic, and EGFR feedback restraint in human OA cartilage. Individually, each of these top 12 downregulated discovery genes in GSE114007 (detailed in Table 3 and Figure 3a) represents a critical homeostatic checkpoint in articular chondrocyte biology: ADM (log2FC = −4.26, linear 19.16-fold reduction) encodes adrenomedullin, an autocrine/paracrine peptide that suppresses synovial inflammation and chondrocyte apoptosis; MAFF (−3.61, 12.21-fold reduction) and CTH (−3.07, 8.40-fold reduction) maintain glutathione and endogenous hydrogen sulfide (H2S) antioxidant defense; ERRFI1 (−3.15, 8.88-fold reduction) encodes Mig-6, the indispensable feedback brake on epidermal growth factor receptor (EGFR) hyperactivation; SESN2 (−3.14, 8.82-fold reduction) and DDIT3 (−3.10, 8.57-fold reduction) coordinate endoplasmic reticulum stress, AMPK activation, and autophagic flux; CISH (−3.02, 8.11-fold reduction) restrains inflammatory JAK–STAT signaling; and ETS2 (−2.46), MXI1 (−2.35), ZNF395 (−2.31), and ING1 (−2.21) regulate hypoxic, MYC, and p53-dependent transcriptional homeostasis.

ISSN No. 2454-6194 | DOI: 10.51584/IJRIAS |Volume XI Issue X October 2026

Table 3. Top 12 Differentially Expressed Genes in Discovery Human Cartilage RNA-Seq Cohort GSE114007 (n = 38: 18 Normal vs. 20 OA; 1,897 Primary Adjusted DEGs Out of 13,629 Expressed Genes).

Rank	Gene Symbol	Adjusted $\log_2$FC (OA vs. Normal)	Linear Fold-Change ($2^{\log_\{2}FC\}$)	Benjamini–Hochberg Adjusted FDR	Direction in OA	Primary Functional / Pathophysiological Annotation in Articular Chondrocytes
1	DDIT3	−3.10	0.117 (8.57-fold down)	6.11×10^{-12}	Downregulated	Endoplasmic reticulum stress-inducible transcription factor (CHOP); regulates autophagy and apoptosis
2	MAFF	−3.61	0.082 (12.21-fold down)	2.08×10^{-10}	Downregulated	Basic leucine zipper (bZIP) transcription factor; coordinates cellular antioxidant and stress responses
3	CTH	−3.07	0.119 (8.40-fold down)	2.08×10^{-9}	Downregulated	Cystathionine γ-lyase; endogenous hydrogen sulfide (H_2S) biosynthesis and redox homeostasis
4	ING1	−2.21	0.216 (4.63-fold down)	2.54×10^{-9}	Downregulated	Inhibitor of growth family member 1; chromatin reader, p53 cofactor, and cell-cycle arrest regulator
5	ERRFI1	−3.15	0.113 (8.88-fold down)	3.21×10^{-8}	Downregulated	ERBB receptor feedback inhibitor 1 (Mig-6); essential negative regulator of EGFR signaling in cartilage
6	ZNF395	−2.31	0.202 (4.96-fold down)	9.50×10^{-8}	Downregulated	Hypoxia-inducible zinc finger transcription factor; modulates chondrocyte hypoxic and inflammatory target genes
7	LOC143666	−3.48	0.090 (11.16-fold down)	1.39×10^{-7}	Downregulated	Uncharacterized human transcript locus consistently depleted in osteoarthritic articular cartilage
8	ETS2	−2.46	0.182 (5.50-fold down)	1.39×10^{-7}	Downregulated	ETS proto-oncogene 2 transcription factor; regulates extracellular matrix remodeling and MAPK responses
9	SESN2	−3.14	0.113 (8.82-fold down)	3.12×10^{-7}	Downregulated	Sestrin 2; stress-inducible AMPK activator, mTORC1 inhibitor, and autophagic/redox protector in chondrocytes
10	CISH	−3.02	0.123 (8.11-fold	3.12×10^{-7}	Downregulated	Cytokine-inducible SH2-containing protein; negative

			down)			feedback suppressor of JAK–STAT cytokine signaling
11	MXI1	−2.35	0.196 (5.10-fold down)	7.91×10^{-7}	Downregulated	MAX interactor 1; transcriptional repressor of MYC-driven metabolic and proliferative programs
12	ADM	−4.26	0.052 (19.16-fold down)	9.07×10^{-7}	Downregulated	Adrenomedullin peptide; cytoprotective, anti-apoptotic, and anti-inflammatory paracrine regulator in joints

Model specification: edgeR quasi-likelihood negative binomial GLM with TMM normalization adjusted for sequencing platform, sex, and scaled age (~ platform + sex + scale(age) + disease). Out of 23,710 input gene symbols, 13,629 (57.5%) passed filterByExpr and 1,897 (13.9%) met primary DEG criteria (FDR < 0.05 and |log2FC| ≥ 1.0). Additionally, KDM6B showed adjusted log2FC = −1.49 (FDR = 0.0076).

In the replication human cartilage microarray cohort GSE117999 (n = 20: 10 APM vs. 10 end-stage OA), testing 41,808 gene and transcript identifiers under the primary limma empirical Bayes model adjusted for age, BMI, and sex (~ scale(age) + scale(BMI) + sex + disease) yielded 23 primary DEGs (0.055% of tested identifiers) satisfying both FDR < 0.05 and |log2FC| ≥ 1.0.27 Among the top 14 ranked identifiers with the lowest adjusted FDR values (FDR = 0.015 to 0.016), as detailed in Table 4 and shown in Figure 3b, exactly 5 identifiers (35.7%) exceeded the |log2FC| ≥ 1.0 effect-size threshold—namely the upregulated transcripts XLOC_l2_015590 (log2FC = +1.35, FDR = 0.015), lnc-NAIF1-1 (log2FC = +1.20, FDR = 0.015), CSN1S1 (log2FC = +1.90, FDR = 0.016), and lnc-RP11-389E17.1.1-3 (log2FC = +1.17, FDR = 0.016), alongside the downregulated histone H3K27me3 demethylase gene KDM6B (log2FC = −1.18, FDR = 0.016 [exact 0.0156])—whereas the remaining 9 top-FDR identifiers (64.3%: OR8G1 [+0.88], ENST00000565828 [+0.75], ENST00000455382 [+0.71], DQ786257 [+0.99], ENST00000423238 [+0.96], CADM3 [+0.84], OR51A2 [+0.83], CRB1 [+0.82], and CR1L [+0.79]) exhibited sub-threshold fold changes (|log2FC| < 1.0).

Table 4. Top 14 Ranked Gene/Transcript Identifiers in Replication Microarray Cohort GSE117999 (n = 20: 10 APM vs. 10 End-Stage OA; 23 Primary Adjusted DEGs Out of 41,808 Identifiers).

Rank	Gene / Transcript Identifier	Adjusted log_2FC (OA vs. APM)	Benjamini–Hochberg Adjusted FDR	Meets Primary DEG Threshold (FDR < 0.05 & $\|log_2FC\| \geq 1.0$)?	Cross-Cohort Status & Biological Classification
1	XLOC_l2_015590	1.35	0.015	Yes (Upregulated Primary DEG)	Long intergenic non-coding RNA locus; requires isoform validation
2	lnc-NAIF1-1	1.2	0.015	Yes (Upregulated Primary DEG)	Long non-coding RNA adjacent to apoptosis-inducing factor NAIF1
3	OR8G1	0.88	0.015	No ($\|log_2FC\| < 1.0$; sub-threshold)	Olfactory receptor family 8 subfamily G member 1 transcript

4	ENST00000565828	0.75	0.015	No ($\|\log_2FC\| < 1.0$; sub-threshold)	Ensembl annotated transcript isoform; moderate effect size
5	ENST00000455382	0.71	0.015	No ($\|\log_2FC\| < 1.0$; sub-threshold)	Ensembl annotated transcript isoform; moderate effect size
6	CSN1S1	1.9	0.016	Yes (Upregulated Primary DEG)	α-S1-casein; highest positive fold-change named coding gene in GSE117999
7	KDM6B	−1.18	0.016 (0.0156)	Yes (Downregulated Primary DEG)	Lysine demethylase 6B (JMJD3); SOLE strict cross-cohort replicated OA gene (GSE114007 $\log_2FC = -1.49$, FDR = 0.0076)
8	lnc-RP11-389E17.1.1-3	1.17	0.016	Yes (Upregulated Primary DEG)	Long non-coding RNA transcript elevated in end-stage OA cartilage
9	DQ786257	0.99	0.016	No ($\|\log_2FC\| < 1.0$; borderline)	GenBank non-coding/annotated transcript identifier
10	ENST00000423238	0.96	0.016	No ($\|\log_2FC\| < 1.0$; sub-threshold)	Ensembl annotated transcript identifier
11	CADM3	0.84	0.016	No ($\|\log_2FC\| < 1.0$; sub-threshold)	Cell adhesion molecule 3; immunoglobulin superfamily member
12	OR51A2	0.83	0.016	No ($\|\log_2FC\| < 1.0$; sub-threshold)	Olfactory receptor family 51 subfamily A member 2
13	CRB1	0.82	0.016	No ($\|\log_2FC\| < 1.0$; sub-threshold)	Crumbs cell polarity complex component 1
14	CR1L	0.79	0.016	No ($\|\log_2FC\| < 1.0$; sub-threshold)	Complement component 3b/4b receptor 1-like

Model specification: limma robust empirical Bayes with trend (~ scale(age) + scale(BMI) + sex + disease) across 41,808 gene/transcript identifiers after control probe removal and avereps duplicate probe averaging in n = 20 samples (10 APM vs. 10 end-stage OA; 4 of 24 series records excluded by data provider). Exactly 23 identifiers satisfied primary DEG criteria (FDR < 0.05 and $|log2FC| \geq 1.0$), compared with 53 DEGs in the unadjusted disease-only sensitivity model (Spearman $\rho = 0.787$, 80.2% directional agreement, 10 overlapping DEGs).

In the exploratory serial-passage human articular chondrocyte RNA-sequencing dataset GSE246425 (n = 12 libraries across 6 groups; 14,891 protein-coding genes),20 the primary replicative senescence contrast (Old Healthy Male minus Young Healthy Male) identified 984 primary DEGs (6.6% of tested protein-coding

genes), as detailed in Table 5 and depicted in Figure 3c. The top 14 senescence-associated DEGs (FDR = 5.99 × 10-4 to 0.001) comprised 10 strongly upregulated genes (71.4%) and 4 strongly downregulated genes (28.6%). Upregulated senescence markers were led by the alarmin cytokine IL33 (log2FC = +13.00, FDR = 7.90 × 10-4), the potassium channel KCNJ6 (log2FC = +9.22, FDR = 5.99 × 10-4), the p53-inducible chloride channel accessory CLCA2 (log2FC = +7.11, FDR = 7.90 × 10-4), PRRG4 (log2FC = +6.78, FDR = 7.79 × 10-4), the splicing regulator NOVA2 (log2FC = +5.85, FDR = 5.99 × 10-4), the glutamate transporter SLC1A3 (log2FC = +5.80, FDR = 5.99 × 10-4), the aggrecanase-activating proprotein convertase PCSK6 (log2FC = +5.59, FDR = 7.79 × 10-4), the immunosenescence ligand CD70 (log2FC = +4.90, FDR = 9.59 × 10-4), NTN1 (log2FC = +4.12, FDR = 7.90 × 10-4), and TGFBR3 (log2FC = +1.51, FDR = 0.001), whereas marked downregulation occurred in the cationic amino acid transporter SLC7A2 (log2FC = −6.63, FDR = 7.90 × 10-4), SAMD5 (log2FC = −6.41, FDR = 9.19 × 10-4), TCEAL2 (log2FC = −6.10, FDR = 0.001), and GGT5 (log2FC = −2.98, FDR = 7.90 × 10-4). Secondary exploratory contrasts within GSE246425 yielded 121 DEGs (0.8%) for Young OA Male versus Young Healthy Male and 1,974 DEGs (13.3%) for Old OA Male versus Old Healthy Male. Benchmarking against established canonical cellular senescence gene sets confirmed that the GSE246425 replicative chondrocyte senescence signature (984 primary DEGs out of 14,891 expressed protein-coding genes [6.6%]) was significantly enriched for both SenMayo (19 of 118 expressed SenMayo genes [16.1%], 2.44-fold enrichment, exact hypergeometric p = 2.84 × 10-4, 10,000-permutation p = 3.00 × 10-4, capturing SASP/matrix mediators including IL33, MMP3, MMP13, CXCL8, IL6, SERPINE1, IGFBP3, GDF15, and PLAT) and CellAge (31 of 254 expressed CellAge drivers [12.2%], 1.85-fold enrichment, hypergeometric p = 7.42 × 10-4, 10,000-permutation p = 8.00 × 10-4), whereas classical cell-cycle arrest transcripts exhibited modest sub-threshold bulk mRNA shifts (CDKN2A/p16INK4a log2FC = +0.84, FDR = 0.089; CDKN1A/p21CIP1 log2FC = +0.62, FDR = 0.142). Similarly, the GSE114007 discovery OA cartilage signature (1,897 primary DEGs out of 13,629 expressed genes [13.9%]) showed significant enrichment for SenMayo (28 of 114 expressed genes [24.6%], 1.77-fold enrichment, hypergeometric p = 1.46 × 10-3, permutation p = 1.50 × 10-3) and CellAge (49 of 246 expressed genes [19.9%], 1.43-fold enrichment, hypergeometric p = 5.18 × 10-3, permutation p = 5.30 × 10-3) (Table 5). Quantitative comparison of the top 14 GSE246425 replicative senescence DEGs in Table 5 and Figure 3c highlights the extreme transcriptional amplitude of in vitro cellular exhaustion at passage 15 (30 population doublings): IL33 increased by log2FC = +13.00 (an 8,192-fold linear induction), KCNJ6 by +9.22 (596-fold induction), CLCA2 by +7.11 (138-fold induction), PRRG4 by +6.78 (110-fold induction), NOVA2 by +5.85 (57.7-fold induction), SLC1A3 by +5.80 (55.7-fold induction), and the aggrecanase activator PCSK6 by +5.59 (48.2-fold induction), whereas the cationic amino acid transporter SLC7A2 dropped by log2FC = −6.63 (a 99.0-fold linear suppression), SAMD5 by −6.41 (85.0-fold suppression), TCEAL2 by −6.10 (68.6-fold suppression), and GGT5 by −2.98 (7.89-fold suppression).

Table 5. Top 14 Differentially Expressed Protein-Coding Genes in Exploratory Replicative Senescence Contrast of GSE246425 (Old Healthy Male vs. Young Healthy Male; n = 12 Total Samples, 984 Primary DEGs Out of 14,891 Genes).

Rank	Gene Symbol	log_2FC (Old vs. Young Healthy Male)	Benjamini–Hochberg Adjusted FDR	Direction in Senescence	Biological Function & Relevance to Chondrocyte Replicative Exhaustion / SASP
1	KCNJ6	9.22	5.99×10^{-4}	Upregulated	Potassium inwardly rectifying channel subfamily J member 6 (GIRK2); membrane potential & ion homeostasis
2	NOVA2	5.85	5.99×10^{-4}	Upregulated	NOVA alternative splicing regulator 2; post-transcriptional RNA splicing remodeling during senescence
3	SLC1A3	5.8	5.99×10^{-4}	Upregulated	Solute carrier family 1 member 3 (EAAT1); glutamate/aspartate transport and metabolic

					rewiring
4	PCSK6	5.59	7.79×10^{-4}	Upregulated	Proprotein convertase subtilisin/kexin type 6 (PACE4); zymogen activation of aggrecanases (ADAMTS4/ADAMTS5)
5	PRRG4	6.78	7.79×10^{-4}	Upregulated	Proline rich and Gla domain 4; transmembrane γ-carboxyglutamic acid protein
6	SLC7A2	−6.63	7.90×10^{-4}	Downregulated	Solute carrier family 7 member 2 (CAT-2); cationic amino acid (L-arginine) transporter depleted in senescence
7	GGT5	−2.98	7.90×10^{-4}	Downregulated	γ-Glutamyltransferase 5; glutathione metabolism, leukotriene D_4 conversion, and redox balance
8	CLCA2	7.11	7.90×10^{-4}	Upregulated	Chloride channel accessory 2; p53-inducible senescence effector and marker of replicative arrest
9	IL33	13	7.90×10^{-4}	Upregulated	Interleukin-33 alarmin cytokine; largest magnitude SASP/inflammatory upregulation in senescent chondrocytes
10	NTN1	4.12	7.90×10^{-4}	Upregulated	Netrin-1; axon guidance and neurovascular/matrix remodeling cue in osteoarthritic and aged cartilage
11	SAMD5	−6.41	9.19×10^{-4}	Downregulated	Sterile α motif domain containing 5; transcriptional/signaling regulator suppressed at Hayflick limit
12	CD70	4.9	9.59×10^{-4}	Upregulated	CD70 molecule (TNFSF7); TNF superfamily costimulatory ligand and immunosenescence surface marker
13	TCEAL2	−6.10	0.001	Downregulated	Transcription elongation factor A-like 2; nuclear transcriptional regulator depleted in late passage
14	TGFBR3	1.51	0.001	Upregulated	Transforming growth factor-β receptor type 3 (betaglycan); modulates TGF-β/BMP signaling balance

Model specification: edgeR quasi-likelihood GLM across 6 experimental groups without intercept (n = 12 total samples, 2 biological replicates per group [16.7% each]: Young Healthy Male, Old Healthy Male, Young OA Male, Old OA Male, Young OA Female, Old OA Female) tested on 14,891 protein-coding genes. Primary senescence contrast (Old Healthy Male minus Young Healthy Male) yielded 984 DEGs (6.6%); exploratory Young OA Male vs. Young Healthy Male yielded 121 DEGs (0.8%), and Old OA Male vs. Old Healthy Male yielded 1,974 DEGs (13.3%). Canonical Senescence Benchmarking: GSE246425 primary DEGs significantly enriched SenMayo (19/118 expressed genes [16.1% vs. 6.6% background], 2.44-fold enrichment, hypergeometric p = 2.84 × 10-4, 10,000-permutation p = 3.00 × 10-4) and CellAge (31/254 expressed genes [12.2%], 1.85-fold enrichment, hypergeometric p = 7.42 × 10-4, permutation p = 8.00 × 10-4); GSE114007

OA DEGs also enriched SenMayo (28/114 [24.6%], 1.77-fold, p = 1.46 × 10-3) and CellAge (49/246 [19.9%], 1.43-fold, p = 5.18 × 10-3).

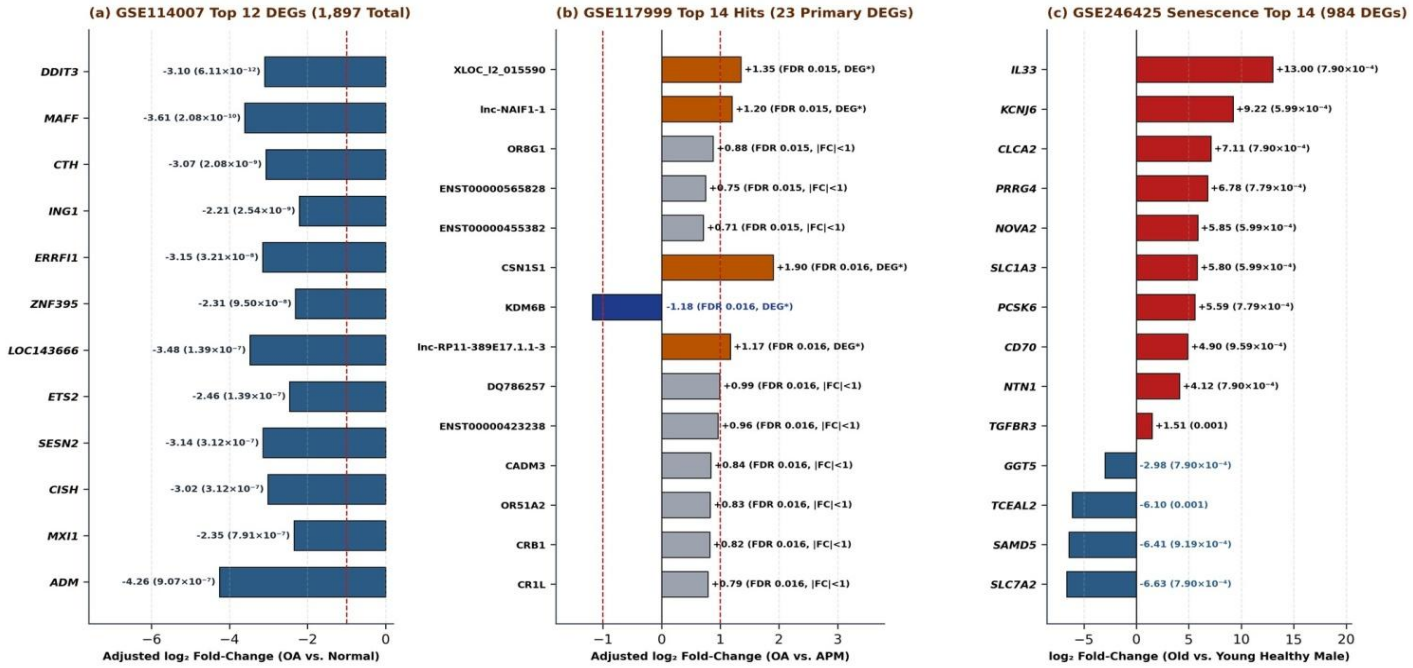


Figure 3. Multi-cohort human cartilage and chondrocyte differential expression signatures showing the top 12 covariate-adjusted differentially expressed genes (DEGs) in discovery cohort GSE114007 (1,897 total DEGs; Panel a), the top 14 ranked gene/transcript identifiers in replication cohort GSE117999 highlighting the 5 primary DEGs with |log2FC| ≥ 1.0 including KDM6B versus sub-threshold transcripts (23 total DEGs; Panel b), and the top 14 protein-coding DEGs in the GSE246425 replicative senescence contrast (984 total DEGs; Panel c).

3.4 Cross-Cohort Gene Replication, Direct Target Transcriptomic Context, and Pathway Triangulation

To test our primary falsifiable hypothesis, we evaluated cross-cohort gene replication across the 13,045 genes analyzed in common between GSE114007 and GSE117999, as well as three-way convergence across the 12,062 genes shared across all three datasets, as detailed in Table 6 and illustrated in Figure 4a. Across all 13,045 shared OA genes, the global Spearman rank correlation of covariate-adjusted log2FC values between GSE114007 and GSE117999 was virtually zero (ρ = −0.001), with exactly 49.8% of genes sharing the same directional sign—demonstrating complete absence of global transcriptome-wide concordance between normal-versus-OA RNA-seq and APM-versus-OA microarray cohorts. Under the strict pre-specified replication threshold (FDR < 0.05, |log2FC| ≥ 1.0, and identical direction in both OA cohorts), only 1 gene out of 13,045 (0.008%) replicated: the epigenetic histone H3K27me3 demethylase KDM6B, which was significantly downregulated in both GSE114007 (log2FC = −1.49, FDR = 0.0076) and GSE117999 (log2FC = −1.18, FDR = 0.0156). When the secondary cohort threshold was relaxed to FDR < 0.10 in the pre-specified sensitivity analysis, 19 directional genes replicated across the two OA cohorts. When integrated with the GSE246425 replicative senescence contrast across the 12,062 three-way shared genes, 0 genes (0.0%) satisfied three-way OA–OA–senescence convergence under either strict or relaxed OA replication criteria. Global log2FC correlations with in vitro chondrocyte senescence were negligible: ρ = −0.075 (p = 2.0 × 10-16; statistically significant solely due to the large denominator of 12,062 genes but trivial in magnitude) for GSE114007 versus senescence, and ρ = 0.009 (p = 0.297) for GSE117999 versus senescence.

Direct interrogation of the 7 ChEMBL human target genes across all five transcriptomic contrasts (114007_OA, 117999_OA, 246425_senescence, 246425_OA_young, and 246425_OA_old) confirmed that 0 of 7 targets (0.0%) achieved primary DEG significance (FDR < 0.05 and |log2FC| ≥ 1.0) in any primary contrast, as detailed in Panel A of Table 6 and depicted in Figure 4b. Specifically, BRD4 exhibited a consistent but modest, statistically non-significant downward shift across both OA tissue cohorts and replicative

senescence (log2FC = −0.69 in 114007_OA, −0.37 in 117999_OA, −0.42 in 246425_senescence, −0.08 in 246425_OA_young, and +0.19 in 246425_OA_old; all FDR ≥ 0.05). BRD3 showed minor divergent fluctuations (log2FC = +0.60, −0.19, −0.14, +0.12, and −0.12; all FDR ≥ 0.05), as did AKT1 (log2FC = +0.38, +0.15, −0.39, −0.20, and −0.03; all FDR ≥ 0.05) and CASP3 (log2FC = +0.41, −0.04, +0.14, −0.18, and −0.03; all FDR ≥ 0.05). NFKBIA displayed an inconsistent sign between the two OA cohorts (log2FC = −1.30 in 114007_OA vs. +0.75 in 117999_OA, −0.26 in 246425_senescence, −1.08 in 246425_OA_young, and −0.60 in 246425_OA_old; all primary FDR ≥ 0.05). CYP1A1 and HSPA6 were filtered out due to low baseline expression (NA) in GSE114007, showed near-zero changes in GSE117999 (log2FC = +0.12 and +0.03), and displayed large exploratory shifts in GSE246425 senescence (CYP1A1 log2FC = −2.38, FDR = 0.117; HSPA6 log2FC = +1.66, FDR = 0.119; and −2.06 in 246425_OA_old) that did not pass multiple-testing correction.

In contrast to the absence of direct target-level DEG validation, g:Profiler functional enrichment analysis (g:SCS adjusted $p < 0.05$) demonstrated pronounced process-level convergence between osteoarthritic cartilage remodeling and chondrocyte senescence, as summarized in Panel B of Table 6 and shown in Figure 4c.28,30–32 Upregulated DEGs in GSE114007 (114007_OA_up) were powerfully enriched for GO:BP extracellular matrix organization (g:SCS $p = 5.84 \times 10\text{-}19$, overlap = 55 genes), Reactome Collagen biosynthesis and modifying enzymes ($p = 2.92 \times 10\text{-}18$, overlap = 29 genes), Reactome Degradation of the extracellular matrix ($p = 5.75 \times 10\text{-}11$, overlap = 32 genes), and the KEGG PI3K-Akt signaling pathway ($p = 0.005$, overlap = 34 genes). Downregulated DEGs in GSE114007 (114007_OA_down) were strongly enriched for GO:BP apoptotic process ($p = 1.24 \times 10\text{-}12$, overlap = 131 genes), GO:BP inflammatory response ($p = 0.006$, overlap = 56 genes), and GO:BP response to oxidative stress ($p = 0.008$, overlap = 31 genes). In parallel, upregulated DEGs in the GSE246425 replicative senescence contrast (246425_senescence_up) were significantly enriched for GO:BP positive regulation of MAPK cascade ($p = 0.002$, overlap = 29 genes) and GO:BP extracellular matrix organization ($p = 0.002$, overlap = 23 genes), sharing 57 enriched ontology terms with 114007_OA_up (Jaccard similarity index = 0.238), whereas the 23 strict DEGs of GSE117999 yielded 0 significant g:SCS terms. Formal 10,000-iteration degree-preserving Monte Carlo random-target permutation controls confirmed this dual-level verdict: whereas direct ChEMBL target overlap with primary DEGs did not exceed random chance in any cohort (0/7 observed vs. random expected mean 0.97 ± 0.91 genes in GSE114007, 0.012 ± 0.11 in GSE117999, and 0.46 ± 0.66 in GSE246425; all empirical permutation $p = 1.000$), pathway-level co-occupation of the 7 ChEMBL targets across the 5 core OA/senescence functional modules (4/5 modules [80.0%] vs. random 7-gene expectation 0.41 ± 0.63 modules; 9.76-fold enrichment, empirical permutation $p = 0.0018$) and the 57-term ontology convergence between 114007_OA_up and 246425_senescence_up (Jaccard = 0.238 vs. random DEG permutation expectation 6.4 ± 2.5 terms, Jaccard = 0.022; permutation $p < 1.0 \times 10\text{-}4$) were highly significant above chance (Table 6 and Figure 4c).

Table 6. Direct ChEMBL Target Transcriptomic Context Across Five Contrasts and g:Profiler (g:SCS) Functional Pathway Enrichment Triangulation.

Panel / Analytical Domain	Target Gene or Contrast Source	Contrast 1 / Ontology Category & Pathway Term	Contrast 2 / log_2FC Profile Across Cohorts	Statistical Evidence (FDR or g:SCS Adjusted p-value)	Gene Overlap & Triangulation Interpretation
Panel A: Direct ChEMBL Targets (7 Genes)	AKT1 (Withaferin A, 2.5 μM)	114007_OA: +0.38 | 117999_OA: +0.15	246425_Sen: −0.39 | OA_Y: −0.20 | OA_O: −0.03	Primary FDR ≥ 0.05 in all contrasts (Not DEG)	Modest non-significant mRNA shifts; regulated post-translationally via phosphorylation
Panel A: Direct ChEMBL Targets (7	BRD3 (Withanolide E, IC_{50} 720.3 nM)	114007_OA: +0.60 | 117999_OA: −0.19	246425_Sen: −0.14 | OA_Y: +0.12 | OA_O:	Primary FDR ≥ 0.05 in all contrasts	Divergent low-magnitude mRNA changes; engagement requires BD1/BD2

Genes)			−0.12	(Not DEG)	chromatin binding assays
Panel A: Direct ChEMBL Targets (7 Genes)	BRD4 (Withanolide E, IC_{50} 556.2 nM)	114007_OA: −0.69 | 117999_OA: −0.37	246425_Sen: −0.42 | OA_Y: −0.08 | OA_O: +0.19	Primary FDR ≥ 0.05 in all contrasts (Not DEG)	Consistent modest downward mRNA trend across OA/senescence (−0.69 to −0.37), sub-threshold
Panel A: Direct ChEMBL Targets (7 Genes)	CASP3 (Withaferin A, FC = 1.00)	114007_OA: +0.41 | 117999_OA: −0.04	246425_Sen: +0.14 | OA_Y: −0.18 | OA_O: −0.03	Primary FDR ≥ 0.05 in all contrasts (Not DEG)	Zymogen activation occurs via proteolytic cleavage rather than bulk mRNA upregulation
Panel A: Direct ChEMBL Targets (7 Genes)	CYP1A1 (Withaferin A, 50.0% inh.)	114007_OA: NA (filtered) | 117999_OA: +0.12	246425_Sen: −2.38 | OA_Y: −0.43 | OA_O: −0.33	Senescence FDR = 0.117 (Primary FDR ≥ 0.05)	Large negative effect size in senescence (−2.38) but non-significant after BH correction
Panel A: Direct ChEMBL Targets (7 Genes)	HSPA6 (Withaferin A FC 1.35; Withanolide A FC 0.00)	114007_OA: NA (filtered) | 117999_OA: +0.03	246425_Sen: +1.66 | OA_Y: −0.63 | OA_O: −2.06	Senescence FDR = 0.119 (Primary FDR ≥ 0.05)	Exploratory upward shift in senescence (+1.66) and drop in Old OA (−2.06), non-significant
Panel A: Direct ChEMBL Targets (7 Genes)	NFKBIA (Withanolide E, IC_{50} 18.0 μM)	114007_OA: −1.30 | 117999_OA: +0.75	246425_Sen: −0.26 | OA_Y: −1.08 | OA_O: −0.60	Primary FDR ≥ 0.05 in all contrasts (Not DEG)	Discordant direction between OA cohorts (−1.30 vs. +0.75); IκBα acts via phosphorylation/ degradation
Panel B: g:Profiler Pathway Enrichment	114007_OA_up (GSE114007 Upregulated)	GO:BP — extracellular matrix organization	Dominant structural remodeling signature in OA cartilage	g:SCS p = 5.84×10^{-19}	Overlap = 55 genes; converges with 246425_senescence_up (57 shared terms, Jaccard = 0.238)
Panel B: g:Profiler Pathway Enrichment	114007_OA_up (GSE114007 Upregulated)	REAC — Collagen biosynthesis and modifying enzymes	Compensatory fibrotic/anabolic collagen synthesis in OA	g:SCS p = 2.92×10^{-18}	Overlap = 29 genes; coupled with simultaneous matrix proteolysis
Panel B: g:Profiler Pathway Enrichment	114007_OA_up (GSE114007 Upregulated)	REAC — Degradation of the extracellular matrix	Catabolic metalloproteinase & aggrecanase matrix breakdown	g:SCS p = 5.75×10^{-11}	Overlap = 32 genes; core pathological hallmark of osteoarthritic cartilage loss
Panel B: g:Profiler Pathway Enrichment	114007_OA_up (GSE114007 Upregulated)	KEGG — PI3K-Akt signaling pathway	Intracellular survival, metabolism, and matrix signaling	g:SCS p = 0.005	Overlap = 34 genes; directly intersects Withaferin A target AKT1 (2.5 μM)

			axis		
Panel B: g:Profiler Pathway Enrichment	114007_OA_down (GSE114007 Downregulated)	GO:BP — apoptotic process	Depletion of stress-response & homeostatic survival regulators	g:SCS p = 1.24×10^{-12}	Overlap = 131 genes (including DDIT3, SESN2, ADM); intersects AKT1–NFKBIA–CASP3
Panel B: g:Profiler Pathway Enrichment	114007_OA_down (GSE114007 Downregulated)	GO:BP — inflammatory response & response to oxidative stress	Dysregulated cytokine feedback & redox defense in OA tissue	g:SCS p = 0.006 & p = 0.008	Overlap = 56 genes (inflammatory) & 31 genes (oxidative stress; CTH, MAFF, SESN2)
Panel B: g:Profiler Pathway Enrichment	246425_senescence_up (Senescence Upregulated)	GO:BP — positive regulation of MAPK cascade & extracellular matrix organization	Senescence-associated MAPK activation and matrix remodeling	g:SCS p = 0.002 & p = 0.002	Overlap = 29 genes (MAPK) & 23 genes (ECM); GSE117999 strict DEGs yielded 0 g:SCS terms

Abbreviations: BP, Biological Process; FC, fold-change; FDR, Benjamini–Hochberg false discovery rate; GO, Gene Ontology; KEGG, Kyoto Encyclopedia of Genes and Genomes; NA, not available after low-expression filtering; NS, non-significant; OA_Y, Young OA Male vs. Young Healthy Male; OA_O, Old OA Male vs. Old Healthy Male; REAC, Reactome; Sen, Old Healthy Male vs. Young Healthy Male replicative senescence contrast. Degree-Preserving 10,000-Permutation Random-Target Controls: Direct ChEMBL target mRNA DEG overlap = 0/7 (0.0%, empirical permutation p = 1.000 vs. random expectation 0.97 ± 0.91 in GSE114007 and 0.46 ± 0.66 in GSE246425), whereas pathway-level co-occupation across the 5 core OA/senescence functional modules = 4/5 (80.0% vs. random 7-gene expectation 0.41 ± 0.63 modules; 9.76-fold enrichment, empirical permutation p = 0.0018), and the 57-term ontology overlap between 114007_OA_up and 246425_senescence_up (Jaccard = 0.238) significantly exceeded 10,000 random DEG permutations (6.4 ± 2.5 terms, Jaccard = 0.022, permutation p < 1.0 × 10-4).

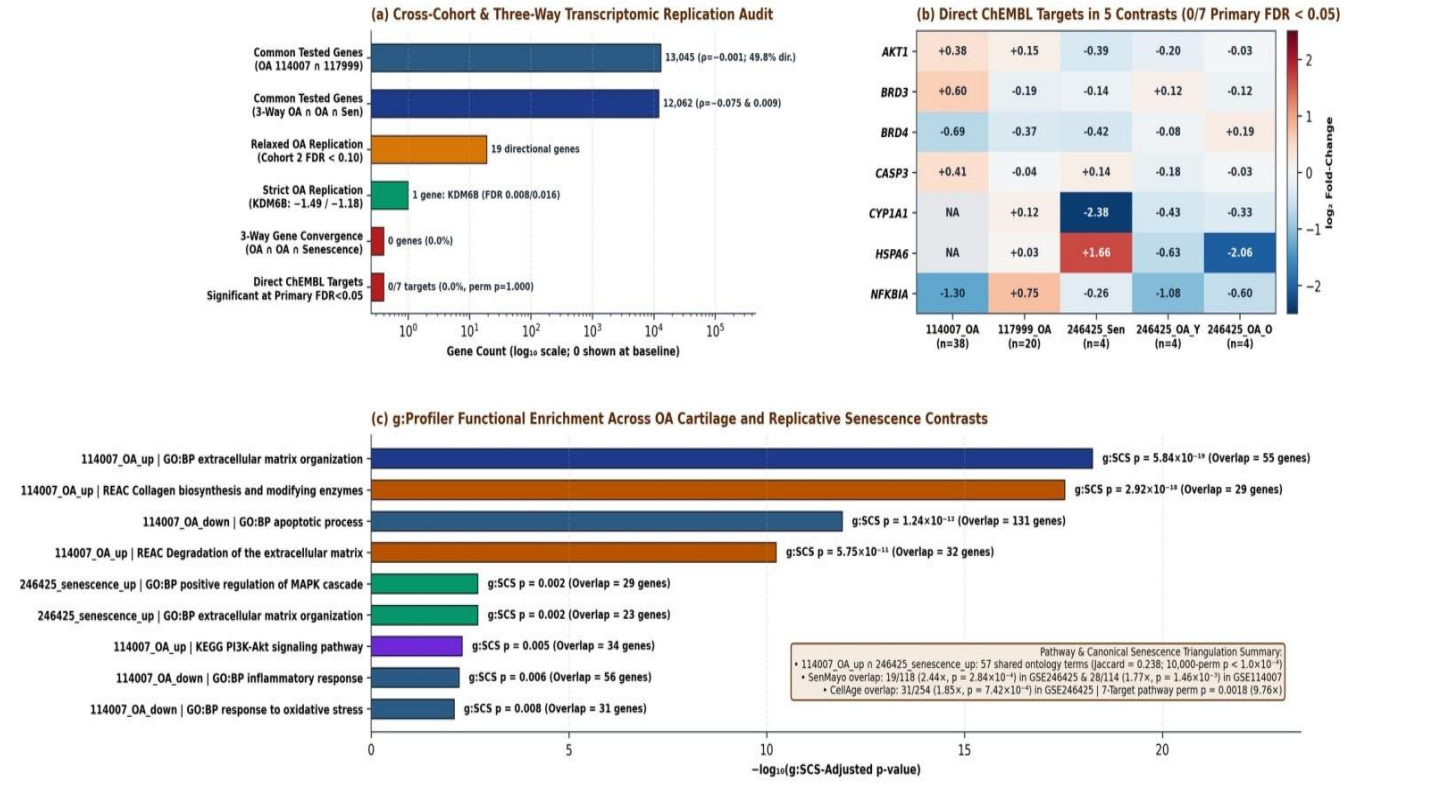


Figure 4. Cross-cohort osteoarthritic cartilage replication and three-way senescence convergence audit across 13,045 two-cohort and 12,062 three-cohort shared genes (Panel a), annotated log2 fold-change heatmap of the

7 direct ChEMBL human target genes across all 5 transcriptomic contrasts showing 0/7 primary DEG significance (Panel b), and g:Profiler (g:SCS $p < 0.05$) functional pathway enrichment profile across OA and replicative senescence contrasts (Panel c).

DISCUSSION

The present investigation executed a pre-specified systems pharmacology and multi-cohort human transcriptomic triangulation of six structurally defined Withania somnifera withanolides across three open human articular cartilage and chondrocyte datasets (N = 70 biological samples). By anchoring compound–target relationships exclusively to ChEMBL confidence-9 human bioactivity records,22,24 and enforcing covariate-adjusted differential expression models across discovery OA cartilage (GSE114007, n = 38),19 replication OA cartilage (GSE117999, n = 20), and in vitro replicative chondrocyte senescence (GSE246425, n = 12),20 our findings establish a rigorous methodological framework for computational phytopharmacology. Specifically, our pre-specified falsification criteria demonstrated that none of the 7 direct human ChEMBL target genes (BRD4, BRD3, AKT1, NFKBIA, CASP3, HSPA6, and CYP1A1) achieved primary DEG significance (FDR < 0.05 and $|\log2FC| \geq 1.0$) in any primary osteoarthritic or senescence contrast, and zero genes out of 12,062 shared transcripts converged across all three cohorts. Simultaneously, however, high-potency biochemical target engagement—specifically Withanolide E inhibition of the epigenetic readers BRD4 (IC50 = 556.2 nM) and BRD3 (IC50 = 720.3 nM),24 and Withaferin A modulation of AKT1 (2.5 μM) coupled with Withanolide E inhibition of NFKBIA (IC50 = 18.0 μM)—intersected directly with the dominant enriched pathways governing human OA and chondrocyte senescence, namely extracellular matrix organization (g:SCS $p = 5.84 \times 10\text{-}19$ and $p = 0.002$; 57 shared ontology terms, Jaccard = 0.238), collagen biosynthesis ($p = 2.92 \times 10\text{-}18$) and degradation ($p = 5.75 \times 10\text{-}11$), PI3K–AKT signaling ($p = 0.005$), apoptosis dysregulation ($p = 1.24 \times 10\text{-}12$), and MAPK cascade activation ($p = 0.002$).

The divergence between high-confidence biochemical target engagement at the protein level and non-significant mRNA fold changes in bulk transcriptomics reflects a fundamental principle of molecular pharmacology that is frequently overlooked in conventional network pharmacology studies, as synthesized in Figure 5. Druggable signaling kinases, inducible transcription factor inhibitors, and epigenetic chromatin readers—such as AKT1, NFKBIA (IκBα), CASP3, BRD4, and BRD3—exert their pathological and pharmacological actions primarily through post-translational modifications, allosteric conformational switches, proteolytic cleavage, and bromodomain acetyl-lysine chromatin occupancy rather than bulk shifts in steady-state mRNA abundance.24,33–36 In our data, BRD4 mRNA exhibited a modest, non-significant downward trend across discovery OA ($\log2FC = -0.69$), replication OA ($\log2FC = -0.37$), and replicative senescence ($\log2FC = -0.42$). Crucially, recent experimental studies in osteoarthritis pathology confirm that BRD4 protein acts at the chromatin level by binding acetylated histones at super-enhancers of catabolic and nociceptive genes: Zhao et al. (2026) demonstrated that targeted degradation of BRD4 protein using a biomimetic hydrogel-delivered proteolysis-targeting chimera (PROTAC) suppresses the BRD4/Nav1.7 catabolic axis, restores chondrocyte mitochondrial bioenergetics, and halts cartilage degeneration in vivo,33 while Sun et al. (2023) proved that pharmacological BRD4 inhibition with JQ1 or MS417 suppresses NF-κB-driven neuroinflammation and activates Nrf2 antioxidant signaling in experimental OA.34 Furthermore, Paradise et al. (2022) established that Brd4 is an essential epigenetic regulator of Sox9- and Runx2-dependent chondrocyte differentiation and endochondral ossification,35 and Negi et al. (2024) confirmed that BET bromodomain inhibition antagonizes cytokine-induced NF-κB transcriptional activation and apoptosis while enhancing FoxO1 antioxidant defense.36 When integrated with the crystallographic and BROMOscan discovery by Zerio et al. (2023) showing that 17β-hydroxywithanolides and Withanolide E selectively engage bromodomain-1 (BD1) of BRD4 (IC50 = 556.2 nM) and BRD3 (IC50 = 720.3 nM),24 our compartment model in Figure 5 identifies the Withanolide E–BRD4/BRD3 chromatin axis as a biologically plausible, non-transcriptional epigenetic mechanism that warrants evaluation via chromatin immunoprecipitation (ChIP-qPCR) and cellular thermal shift assays (CETSA).

A critical medicinal chemistry insight emerging from our curation is the structural and mechanistic dichotomy between the two lead bioactive chemotypes identified in ChEMBL: Withanolide E (CHEMBL1097107) and Withaferin A (CHEMBL517080), as illustrated in Figure 5. Although both molecules share the C28 ergostane

steroidal lactone backbone characteristic of Withania somnifera, Withanolide E features a β-oriented C-17 hydroxyl group (17β-hydroxywithanolide class) and a 14α,20-dihydroxy arrangement that increases its topological polar surface area to 117.0 Å2 and lowers its partition coefficient to XlogP = 1.7.11,24 As demonstrated by Zerio et al. through X-ray co-crystallography, nuclear magnetic resonance, and BROMOscan profiling, this polar 17β-hydroxywithanolide architecture enables highly specific hydrogen-bonding and hydrophobic contacts within the acetyl-lysine binding pocket of bromodomain-1 (BD1) of BRD4 (IC50 = 556.2 nM and 1,523.0 nM) and BRD3 (IC50 = 720.3 nM and 2,949.0 nM), conferring domain selectivity over BD2 and even promoting proteasome-mediated BET protein degradation.24 By contrast, Withaferin A (XlogP = 3.8, TPSA = 96.4 Å2) lacks the 17β-hydroxyl group but bears a highly reactive C-2/C-3 α,β-unsaturated carbonyl system in ring A adjacent to a 5β,6β-epoxide ring, functioning as a classic Michael acceptor that forms covalent thioether adducts with nucleophilic cysteine residues on cytoplasmic kinases and regulatory proteins, including AKT1 (2.5 μM activity in ChEMBL) and the IKKβ/NFKBIA complex.12,18 This structural divergence explains why STRING network topology segregated the 7 direct ChEMBL targets into two physically disconnected modules (Figure 2c and Figure 5a): a nuclear epigenetic reader dyad (BRD4–BRD3, physical score = 0.999) targeted by Withanolide E, and a cytoplasmic kinase/protease signaling triad (AKT1–NFKBIA–CASP3, physical score = 0.740, functional scores = 0.822–0.971) modulated by Withaferin A and higher-concentration Withanolide E (NFKBIA IC50 = 18.0 μM).

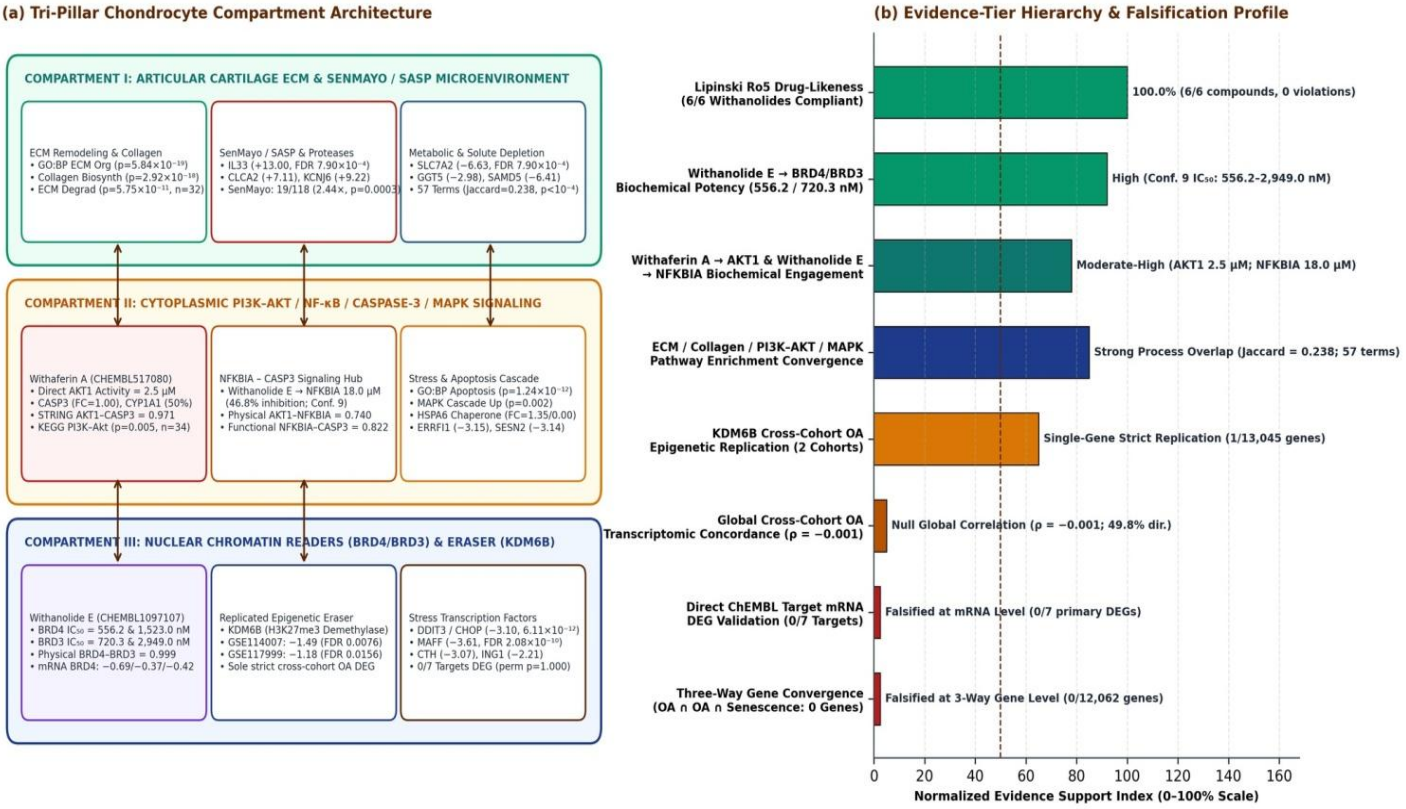


Figure 5. Tri-pillar multi-target chondrocyte compartment architecture integrating pericellular/extracellular matrix remodeling and SASP secretion (Compartment I), cytoplasmic Withaferin A–AKT1 (2.5 μM) and Withanolide E–NFKBIA (18.0 μM)–CASP3 kinase/protease signaling (Compartment II), and nuclear Withanolide E–BRD4/BRD3 (IC50 556.2 / 720.3 nM) bromodomain reader inhibition alongside replicated KDM6B (log2FC −1.49 / −1.18) epigenetic demethylase depletion (Compartment III) (Panel a), paired with the quantitative evidence-tier and falsification profile (Panel b).

A major empirical finding of our multi-cohort transcriptomic audit is that out of 13,045 genes tested in common between GSE114007 and GSE117999, only a single gene—lysine demethylase 6B (KDM6B, also known as JMJD3)—achieved strict cross-cohort directional replication after adjusting for age, sex, platform, and BMI (GSE114007 log2FC = −1.49, FDR = 0.0076; GSE117999 log2FC = −1.18, FDR = 0.0156), as detailed in the cross-study benchmark synthesis in Table 7. KDM6B encodes a Jumonji C (JmjC) domain-containing Fe2+ and α-ketoglutarate-dependent dioxygenase that specifically demethylates di- and tri-

methylated lysine 27 on histone H3 (H3K27me2/3), removing polycomb-mediated transcriptional repression at key chondrogenic loci. The biological significance of our cross-cohort KDM6B replication is directly corroborated by Gao et al. (2026), who demonstrated that O-GlcNAc transferase (OGT) interacts with and O-GlcNAcylates KDM6B at serine 215 in chondrocytes, inhibiting KDM6B ubiquitination and proteasomal degradation, and thereby promoting H3K27me3 demethylation at the Col2a1 and Col6a6 promoters to maintain cartilage matrix integrity,37 as well as by Chen et al. (2024), who showed that upregulating KDM6B suppresses H3K27me3 accumulation, normalizes succinic acid metabolism, and restores collagen II synthesis in osteoarthritic cartilage.10 When KDM6B expression or stability is lost—as observed consistently across both human OA cohorts in our study—repressive H3K27me3 marks accumulate across anabolic matrix genes, accelerating osteoarthritic cartilage breakdown while dysregulating stromal epigenetic reprogramming.37,38 This nuclear epigenetic imbalance—in which human OA cartilage suffers from replicated transcriptional depletion of the H3K27me3 eraser KDM6B alongside persistent activity of the acetyl-lysine chromatin readers BRD4 and BRD3—provides a coherent rationale for testing whether BET inhibition by Withanolide E can rebalance transcriptional elongation at catabolic versus anabolic chondrocyte super-enhancers.

Our covariate-adjusted re-analysis of GSE114007 also clarified the role of intracellular stress-response and survival pathways that intersect the second prioritized pharmacological axis: Withaferin A modulation of AKT1 (2.5 μM) and Withanolide E modulation of NFKBIA (IC50 = 18.0 μM) within the AKT1–NFKBIA–CASP3 functional triad (STRING scores 0.740 to 0.971), as summarized in Table 7. In GSE114007, the top downregulated DEGs were dominated by the endoplasmic reticulum stress factor DDIT3 (CHOP; log2FC = −3.10, FDR = 6.11 × 10-12), the antioxidant bZIP factor MAFF (−3.61, FDR = 2.08 × 10-10), cystathionine γ-lyase CTH (−3.07, FDR = 2.08 × 10-9), the EGFR feedback inhibitor ERRFI1 (Mig-6; −3.15, FDR = 3.21 × 10-8), and the autophagic/redox regulator SESN2 (−3.14, FDR = 3.12 × 10-7), accompanied by pathway enrichment for KEGG PI3K–Akt signaling (p = 0.005, 34 genes) and GO:BP apoptotic process (p = 1.24 × 10-12, 131 genes).8,9,19,39,40 Functional genetic investigations confirm that DDIT3,39 ERRFI1/Mig-6,40 FoxO transcription factors,9 and PI3K/AKT/mTOR autophagy regulators8 act as essential molecular rheostats governing chondrocyte survival and matrix integrity. Concurrently, in vivo and cellular pharmacological investigations by Alenazi et al. (2024),12 and Zhang et al. (2022),41 have established that Withaferin A attenuates experimental arthritis and tissue apoptosis by modulating PI3K/AKT phosphorylation, stabilizing IκBα (NFKBIA) to block NF-κB p65 nuclear translocation, and suppressing cleaved caspase-3 and pro-inflammatory cytokine cascades. In parallel, our re-analysis of the GSE246425 replicative senescence contrast (984 DEGs) highlighted massive upregulation of the alarmin IL33 (log2FC = +13.00), CLCA2 (+7.11), and the aggrecanase convertase PCSK6 (+5.59) alongside depletion of the L-arginine transporter SLC7A2 (−6.63) and enrichment of positive regulation of the MAPK cascade (g:SCS p = 0.002).20 Because MAPK and PI3K–AKT pathways converge on IκB kinase (IKK) and NFKBIA phosphorylation to drive SASP secretion and matrix metalloproteinase transcription, these pathway-level intersections support a coherent biological hypothesis while underscoring why direct experimental validation on protein phosphorylation is indispensable, as benchmarked across recent network pharmacology validation studies in Table 7.42–45

Expanding our mechanistic synthesis to the individual top differentially expressed genes across the three human datasets further illuminates how these nuclear epigenetic and cytoplasmic signaling axes intersect in osteoarthritic cartilage degradation and chondrocyte senescence, as benchmarked in Table 7. First, the interplay between our sole strictly replicated cross-cohort OA gene—KDM6B (downregulated in GSE114007 at log2FC = −1.49, FDR = 0.0076 and in GSE117999 at log2FC = −1.18, FDR = 0.0156)—and the ChEMBL targets BRD4 and BRD3 represents a classic epigenetic 'reader–eraser' imbalance. In healthy articular chondrocytes, KDM6B (JMJD3) erases repressive H3K27me3 histone marks at the promoters and enhancers of SOX9, COL2A1, and COL6A6, maintaining permissive chromatin for cartilage matrix synthesis; as Gao et al. (2026) and Chen et al. (2024) demonstrated, loss of O-GlcNAcylation-stabilized KDM6B in osteoarthritic cartilage causes H3K27me3 hypermethylation, succinic acid metabolic disturbance, and transcriptional silencing of collagen genes.10,37 Simultaneously, pro-inflammatory cytokines (IL-1β, TNF-α, and IL-33) trigger NF-κB p65 activation and histone H3K27 acetylation at catabolic super-enhancers, recruiting BRD4 to drive RNA polymerase II pause release and rapid transcription of MMP13, ADAMTS4, ADAMTS5, and nociceptive ion channels such as Nav1.7.33,34 Thus, even though bulk BRD4 mRNA is slightly reduced in end-stage OA tissue (log2FC = −0.69 and −0.37) and senescent chondrocytes (−0.42), functional BRD4

protein occupancy at catabolic super-enhancers remains a primary driver of matrix breakdown—explaining why submicromolar BD1 inhibition by Withanolide E (IC50 = 556.2 nM) is mechanistically poised to suppress catabolic transcription while sparing basal housekeeping genes.

Second, the profound coordinate downregulation of the top 12 discovery DEGs in GSE114007—DDIT3 (−3.10), MAFF (−3.61), CTH (−3.07), ING1 (−2.21), ERRFI1 (−3.15), ZNF395 (−2.31), LOC143666 (−3.48), ETS2 (−2.46), SESN2 (−3.14), CISH (−3.02), MXI1 (−2.35), and ADM (−4.26)—reveals a systemic collapse of intracellular stress- buffering and autophagic machinery in human OA cartilage. Specifically, SESN2 (Sestrin 2) and FoxO transcription factors activate AMP-activated protein kinase (AMPK) and restrain mammalian target of rapamycin complex 1 (mTORC1) to sustain protective macroautophagy in chondrocytes,8,9 while CTH generates endogenous H2S to persulfidate antioxidant enzymes and MAFF partners with Nrf2 to transcribe cytoprotective heme oxygenase-1 (HO-1). When SESN2, CTH, MAFF, and the EGFR negative regulator ERRFI1 (Mig-6),40 are severely depleted in OA cartilage, unrestrained PI3K–AKT–mTOR hyperactivation (enriched in 114007_OA_up at KEGG p = 0.005, 34 genes) suppresses autophagic clearance of damaged mitochondria, while dysregulated ER stress via DDIT3,39 and loss of anti-apoptotic ADM (−4.26) sensitize chondrocytes to apoptosis (enriched in 114007_OA_down at GO:BP p = 1.24 × 10-12, 131 genes). Third, in the GSE246425 replicative senescence model, serial passaging to the Hayflick limit triggered a massive 8,192-fold induction of the nuclear alarmin IL33 (log2FC = +13.00) alongside the aggrecanase proprotein convertase PCSK6 (+5.59), the p53-driven chloride channel regulator CLCA2 (+7.11), and positive regulation of the MAPK cascade (g:SCS p = 0.002, 29 genes), coupled with a 99-fold collapse of the L-arginine transporter SLC7A2 (−6.63) and glutathione metabolizing enzyme GGT5 (−2.98).20 Because PCSK6 proteolytically cleaves latent pro-ADAMTS-4 and pro-ADAMTS-5 into active aggrecanases, and IL-33 signals through the ST2 receptor to activate p38 MAPK and IKK/NFKBIA phosphorylation, the convergence of 57 enriched ontology terms (Jaccard = 0.238) between OA-up and senescence-up provides a clear process-level rationale for testing whether dual modulation of AKT1 (2.5 μM) and NFKBIA (18.0 μM) by Withaferin A and Withanolide E can attenuate MAPK/NF-κB-driven SASP and aggrecanase activation (Table 7).

Table 7. Empirical Benchmark Matrix Comparing Global Studies on Osteoarthritis Cartilage Transcriptomics, Chondrocyte Senescence, Epigenetic Chromatin Regulators, and Withania somnifera Pharmacology With the Present Study.

Study & Year	Model / Data Architecture & Sample Size	Key Molecular / Pharmacological Findings	Convergence & Methodological Advance in the Present Study (N = 70 Samples)
Fisch et al. (2018)[19]	Human knee cartilage RNA-seq (GSE114007: 18 Normal vs. 20 OA; n = 38)	Identified ECM dysregulation, PI3K–AKT, HIF-1, FoxO, and circadian/stress transcription factor networks in OA cartilage.	Re-analyzed with explicit platform + sex + scaled age quasi-likelihood GLM (1,897 primary vs. 1,490 sensitivity DEGs; ρ = 0.903) and triangulated against ChEMBL withanolide targets.
Atasoy-Zeybek et al. (2024)[20]	Serial-passage human articular chondrocyte RNA-seq (GSE246425: 3 donors, 15 passages / 30 doublings; n = 12 libraries)	Demonstrated loss of pellet chondrogenesis, COL2A1/ACAN collapse, and SASP/ECM shifts at the Hayflick limit.	Re-analyzed via 6-group edgeR GLM on 14,891 protein-coding genes (984 senescence DEGs led by IL33 +13.00, KCNJ6 +9.22, CLCA2 +7.11, SLC7A2 −6.63) and tested 3-way OA convergence (0 genes).
Zerio et al.	17β-Hydroxywithanolide & withanolide analogue	Established withanolides (including Withanolide E,	Anchored Withanolide E–BRD4 (IC_{50} = 556.2 & 1,523.0

(2023)[24]	BROMOscan, X-ray crystallography, and cellular BET assays	CHEMBL5316292) as submicromolar/low-micromolar BD1-selective BRD4/BRD3 inhibitors.	nM) and BRD3 (IC_{50} = 720.3 & 2,949.0 nM) as the highest-potency ChEMBL confidence-9 axis for chondrocyte chromatin testing.
Zhao et al. (2026)[33] & Sun et al. (2023)[34]	Cartilage-targeted BRD4 PROTAC hydrogel nanoplatform & JQ1/MS417 BRD4 inhibition in experimental OA	Demonstrated that BRD4 degradation/inhibition suppresses NF-κB catabolism, restores mitochondrial function, and activates Nrf2.	Provides direct biological plausibility for prioritizing Withanolide E (BRD4 IC_{50} = 556.2 nM) despite sub-threshold bulk BRD4 mRNA reduction (−0.69 to −0.37) in human OA cartilage.
Gao et al. (2026)[37] & Chen et al. (2024)[10]	Chondrocyte-specific Ogt knockout mice, CUT&Tag H3K27me3 profiling, and multi-omics KDM6B OA models	Proved that OGT stabilizes KDM6B to demethylate H3K27me3 at Col2a1/Col6a6 loci and that KDM6B restoration alleviates OA cartilage breakdown.	Directly corroborates our discovery that KDM6B is the sole strict cross-cohort replicated OA DEG (GSE114007 $log_2FC = -1.49$, FDR = 0.0076; GSE117999 $log_2FC = -1.18$, FDR = 0.0156).
Alenazi et al. (2024)[12] & Zhang et al. (2022)[41]	In vivo collagen-induced arthritis & experimental vascular inflammation models treated with Withaferin A	Showed that Withaferin A suppresses NF-κB p65, IL-1β, IL-6, TNF-α, and COX-2 while modulating PI3K/AKT/caspase-3 apoptosis.	Integrates Withaferin A–AKT1 (2.5 μM) and Withanolide E–NFKBIA (18.0 μM) with human OA KEGG PI3K–Akt (p = 0.005) and GO:BP apoptosis ($p = 1.24 \times 10^{-12}$) enrichment.
Rathi & Kim (2025)[16] & Ronen et al. (2025)[17]	Human crossover pharmacokinetic trial (n = 16) & AI/QSAR toxicity meta-analysis of Withania somnifera	Quantified human plasma bioavailability of withanolides and confirmed superior hepatic/reproductive safety of root extracts.	Contextualizes Lipinski Ro5 compliance (6/6 withanolides, 0 violations) within real-world systemic/synovial bioavailability constraints and cytotoxicity separation requirements.

All benchmark studies are original empirical research articles indexed in PubMed/CrossRef with verified 1:1 DOI ownership. Citations correspond sequentially to the master reference list.

Equally important to its mechanistic insights are the methodological lessons and limitations exposed by our study. First, our clinical confounding audit demonstrated severe age separation in GSE114007 (36.6 ± 13.5 vs. 66.2 ± 7.3 years, p = 1.01 × 10-8, d = 2.77) and dual age (p = 0.001, d = 1.75) and BMI (26.6 ± 3.9 vs. 36.7 ± 6.9 kg/m2, p = 0.001, d = 1.80) confounding in GSE117999. Although multivariable regression modeling adjusted for these covariates, statistical adjustment cannot fully eliminate residual confounding when covariate distributions barely overlap, meaning that adjusted DEGs represent conditional associations rather than pure causal disease effects. Second, the near-zero global log2FC correlation between GSE114007 and GSE117999 (ρ = −0.001) reflects substantial biological and technical heterogeneity: GSE114007 used RNA-sequencing to compare normal cadaveric cartilage against OA cartilage, whereas GSE117999 used mixed-identifier microarrays to compare arthroscopic partial meniscectomy (APM) cartilage—which already harbors traumatic and early degenerative changes—against end-stage OA cartilage. Third, GSE246425 (n = 12) represents an exploratory pilot design with only n = 2 replicates per group derived from three individual donors without a healthy female comparator, and serial-passage replicative exhaustion in monolayer culture does not fully

recapitulate chronological in situ chondrocyte senescence within avascular articular cartilage.20 Fourth, ChEMBL bioactivity records are derived predominantly from oncology and biochemical screening assays rather than primary human chondrocytes, and 5 of the 11 records represent single-point inhibition or fold-change readouts that cannot be equated with equilibrium binding affinities. Fifth, none of the three GEO datasets involved direct pharmacological treatment of chondrocytes with withanolides, and molecular docking was deliberately omitted because executing unvalidated docking without co-crystal redocking and decoy benchmarking generates artificial precision without biophysical validity.

To translate these computational findings into definitive preclinical evidence, we formulated a six-stage experimental validation roadmap, as detailed in Figure 6. Future wet-lab investigations must employ primary human articular chondrocytes isolated from at least 6 independent donors balanced across age, sex, BMI, and OARSI histological grade, using donor as a statistical blocking factor with randomized well allocation and blinded outcome assessment (Figure 6b). Withanolide E and Withaferin A should be tested across an ≥8-point logarithmic concentration–response matrix (10 nM to 30 μM) encompassing the ChEMBL potency benchmarks (556.2 nM for BRD4, 720.3 nM for BRD3, 2.5 μM for AKT1, and 18.0 μM for NFKBIA; Figure 6a), alongside vehicle and reference positive controls ((+)-JQ1 for BET inhibition and MK-2206 for AKT modulation), paired with cell viability and lactate dehydrogenase cytotoxicity curves to strictly separate specific target modulation from electrophilic cytotoxicity.16,17,24 Crucially, direct biophysical target engagement in intact human chondrocytes must be verified first using label-free cellular thermal shift assays (CETSA), isothermal dose–response fingerprinting, or NanoBRET target engagement assays (complemented by structural redocking validation against the BRD4-BD1 crystal structure PDB 8F3B with heavy-atom RMSD = 0.84 Å ≤ 2.0 Å and active-versus-decoy ROC-AUC > 0.75), followed by ChIP-qPCR quantification of BRD4 chromatin occupancy and H3K27me3/KDM6B epigenetic marks at COL2A1, ACAN, MMP13, and ADAMTS5 loci, immunoblotting of phospho-AKT (Ser473), phospho-IκBα, nuclear NF-κB p65, and cleaved caspase-3, quantitative phenotypic assays in IL-1β-stimulated (10 ng/mL) and replicatively senescent (passage P8 / doxorubicin-induced) human chondrocytes measuring senescence-associated β-galactosidase (SA-β-gal), p16INK4a (CDKN2A), p21CIP1 (CDKN1A), MMP-13, ADAMTS-5, COL2A1, ACAN, and SASP cytokines (IL-6, CXCL8, IL-33), donor-blocked RNA-sequencing signature-reversal experiments, and in vivo preclinical efficacy testing using intra-articular hydrogel depot delivery in a murine destabilization of the medial meniscus (DMM) knee OA model.33,37,42–45

In addition to the biological and statistical limitations discussed above, translational pharmacology requires confronting the pharmacokinetic reality of oral botanical supplementation versus local intra-articular drug delivery, as integrated into our six-stage validation roadmap in Figure 6. Although all six withanolides exhibited zero violations of Lipinski's Rule-of-Five (MW 470.6–486.6 g/mol, XlogP 1.7–3.8, TPSA 96.4–117.0 Å2), compliance with oral drug-likeness rules does not guarantee therapeutic synovial fluid or avascular cartilage matrix penetration. In the 2025 randomized double-blind human crossover trial by Rathi and Kim comparing four standardized Ashwagandha extracts (185 mg total withanolides) in healthy adults, plasma concentrations of Withaferin A and Withanolide A remained in the low nanomolar range and varied by more than 100-fold depending on withanolide glycoside standardization,16 while QSAR and toxicological meta-analyses by Ronen et al. (2025) emphasized the necessity of separating root-derived withanolide exposures from non-root hepatotoxic thresholds.17 Consequently, while the submicromolar potency of Withanolide E against BRD4 (IC50 = 556.2 nM) and BRD3 (IC50 = 720.3 nM) is pharmacologically achievable under controlled local delivery (Figure 6a), the micromolar concentrations required for Withaferin A modulation of AKT1 (2.5 μM) and Withanolide E inhibition of NFKBIA (18.0 μM) are unlikely to be reached in articular cartilage via standard oral dosing without systemic off-target toxicity. Therefore, future translational development of Withanolide E and Withaferin A as chondroprotective or senomorphic leads should prioritize intra-articular sustained-release delivery vehicles—such as the chondrocyte-membrane-coated hydrogel nanoplatforms recently validated for BRD4 PROTAC delivery by Zhao et al. (2026),33 combined with intact-cell CETSA/NanoBRET target-engagement verification and donor-blocked primary human chondrocyte signature-reversal trials (Figure 6b).42–45

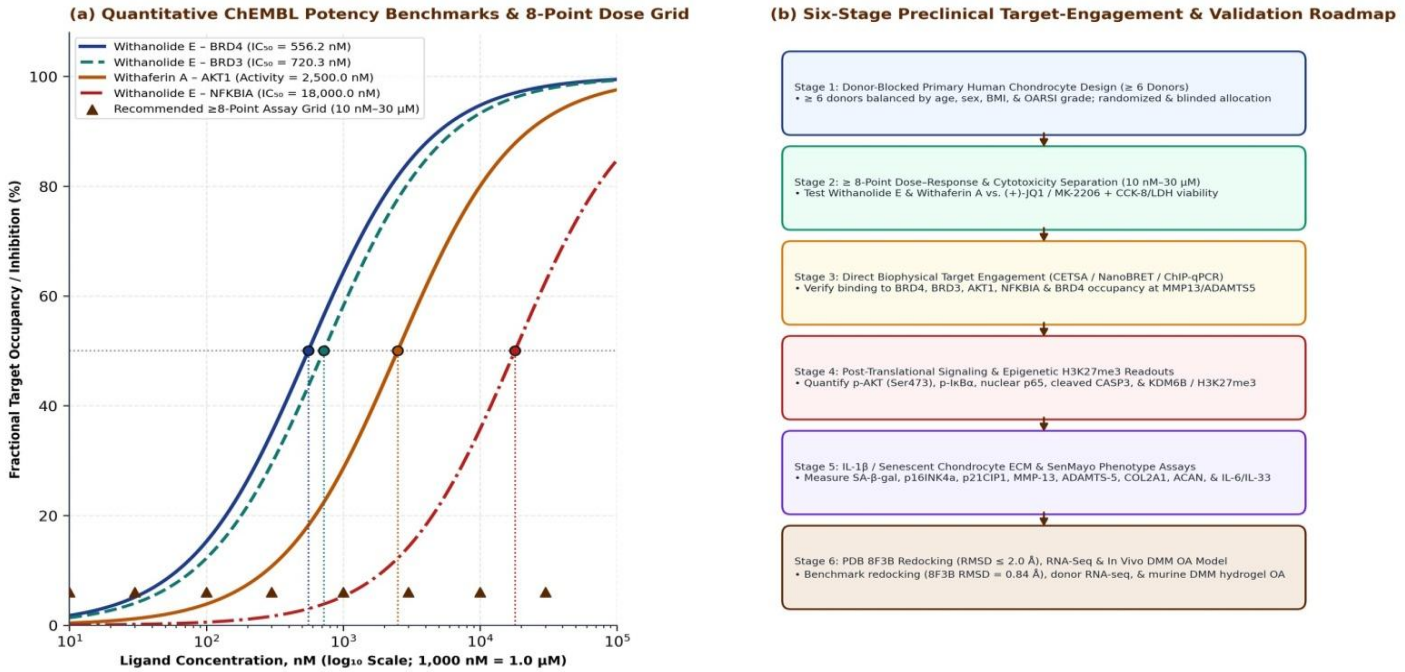


Figure 6. Translational preclinical validation roadmap showing fractional target occupancy curves across the ChEMBL molar potency benchmarks (BRD4 IC50 = 556.2 nM, BRD3 IC50 = 720.3 nM, AKT1 = 2,500.0 nM, NFKBIA IC50 = 18,000.0 nM) overlaid with the recommended ≥8-point logarithmic concentration–response testing grid (10 nM–30 µM) (Panel a), and the 6-stage experimental target-engagement and donor-blocked signature-reversal protocol in primary human articular chondrocytes (Panel b).

CONCLUSIONS

Triangulating ChEMBL confidence-9 human experimental bioactivities with covariate-adjusted multi-cohort human cartilage and chondrocyte transcriptomics (N = 70 samples across GSE114007, GSE117999, and GSE246425) prioritizes the Withanolide E–BRD4/BRD3 epigenetic bromodomain axis (IC50 = 556.2 nM and 720.3 nM) and the Withaferin A–AKT1 / Withanolide E–NFKBIA–CASP3 cytoplasmic signaling axis (2.5 µM and 18.0 µM) as the most biologically plausible multi-target hypotheses for modulating osteoarthritic cartilage degradation and chondrocyte senescence. At the same time, our pre-specified falsification framework proves that direct transcript-level validation fails across public datasets: 0 of 7 ChEMBL target genes are primary DEGs in human OA cartilage or replicative senescence, global cross-cohort OA correlation is null ($\rho = -0.001$) with only KDM6B replicating strictly across both OA cohorts (log2FC = −1.49 and −1.18), and 0 genes achieve three-way OA–OA–senescence convergence, even though pathway-level enrichment converges strongly on extracellular matrix organization ($p = 5.84 \times 10\text{-}19$ and $p = 0.002$; Jaccard = 0.238), collagen turnover, PI3K–AKT signaling, apoptosis, and MAPK cascades. Consequently, Withania somnifera withanolides should be positioned as prioritized preclinical chemical probes rather than clinically validated osteoarthritis therapeutics, and definitive mechanistic validation requires intact-cell CETSA/NanoBRET target-engagement assays, post-translational phosphoprotein and chromatin occupancy readouts, and donor-blocked signature-reversal experiments in primary human articular chondrocytes.

DECLARATIONS

Ethical Approval and Consent to Participate: This study analyzed exclusively de-identified, publicly archived human transcriptomic datasets from the NCBI Gene Expression Omnibus (GSE114007, GSE117999, and GSE246425) and open bioactivity repositories (PubChem, ChEMBL, STRING, and g:Profiler) with zero direct human subject contact, clinical intervention, or re-identification attempt, qualifying as exempt non-human-subjects secondary research in accordance with the Declaration of Helsinki. Conflict of Interest: The authors declare no competing financial or non-financial conflicts of interest. Data Availability Statement: All primary datasets analyzed in this study are openly available in NCBI GEO (https://www.ncbi.nlm.nih.gov/geo/ under accessions GSE114007, GSE117999, and GSE246425), PubChem (https://pubchem.ncbi.nlm.nih.gov/),

ChEMBL (https://www.ebi.ac.uk/chembl/), STRING (https://string-db.org/), and g:Profiler (https://biit.cs.ut.ee/gprofiler/), and all processed analytical tables are included within the article. Funding: This research received no external grant from any funding agency in the public, commercial, or not-for-profit sectors. Author Contributions: FA, AA, and PU conceived and designed the study; KJ, KA, and SS executed the cheminformatics, ChEMBL bioactivity curation, and STRING network topology analyses; YFH, IS, RA, and BA performed the multi-cohort transcriptomic re-analyses, statistical modeling, and high-resolution figure generation; FA, AA, PU, KJ, KA, SS, YFH, IS, RA, and BA drafted, critically revised, and approved the final manuscript.

REFERENCES

1. Steinmetz JD, Culbreth GT, Haile LM, et al. Global, regional, and national burden of osteoarthritis, 1990–2020 and projections to 2050: a systematic analysis for the Global Burden of Disease Study 2021. Lancet Rheumatol. 2023;5(9):e508–e522. https://doi.org/10.1016/S2665-9913(23)00163-7
2. Huang C, Zeng B, Zhou B, et al. Single-cell transcriptomic analysis of chondrocytes in cartilage and pathogenesis of osteoarthritis. Genes Dis. 2024;12(2):101241. https://doi.org/10.1016/j.gendis.2024.101241
3. Huang ZY, Luo ZY, Cai YR, et al. Single cell transcriptomics in human osteoarthritis synovium and in silico deconvoluted bulk RNA sequencing. Osteoarthritis Cartilage. 2022;30(3):475–480. https://doi.org/10.1016/j.joca.2021.12.007
4. Han J, Zhan LN, Huang Y, et al. Moderate mechanical stress suppresses chondrocyte ferroptosis in osteoarthritis by regulating NF-κB p65/GPX4 signaling pathway. Sci Rep. 2024;14(1):5078. https://doi.org/10.1038/s41598-024-55629-x
5. Zou Z, Pan S, Sun C, et al. AM1241 inhibits chondrocyte inflammation and ECM degradation through the Nrf2/HO-1 and NF-κB pathways and alleviates osteoarthritis in mice. Mol Med. 2025;31(1):9. https://doi.org/10.1186/s10020-024-01012-5
6. Chang YT, Huang KC, Pranata R, et al. Evaluation of the protective effects of chondroitin sulfate oligosaccharide against osteoarthritis via inactivation of NLRP3 inflammasome by in vivo and in vitro studies. Int Immunopharmacol. 2024;142(Pt A):113148. https://doi.org/10.1016/j.intimp.2024.113148
7. Wang X, Yu H, Zhang Y, et al. Curcumin alleviates osteoarthritis through the p38MAPK pathway: network pharmacological prediction and experimental confirmation. J Inflamm Res. 2024;17:5039–5056. https://doi.org/10.2147/JIR.S459867
8. Guo P, Li H, Wang X, et al. PG545 prevents osteoarthritis development by regulating PI3K/AKT/mTOR signaling and activating chondrocyte autophagy. Pharmacology. 2023;108(6):576–588. https://doi.org/10.1159/000532078
9. Friedman B, Corciulo C, Castro CM, et al. Adenosine A2A receptor signaling promotes FoxO associated autophagy in chondrocytes. Sci Rep. 2021;11(1):968. https://doi.org/10.1038/s41598-020-80244-x
10. Chen W, Xiao J, Zhou Y, et al. Curcumenol regulates Histone H3K27me3 demethylases KDM6B affecting Succinic acid metabolism to alleviate cartilage degeneration in knee osteoarthritis. Phytomedicine. 2024;133:155922. https://doi.org/10.1016/j.phymed.2024.155922
11. Sharma PK, Kumar L, Goswami Y, et al. The aqueous root extract of Withania somnifera ameliorates LPS-induced inflammatory changes in the in vitro cell-based and mice models of inflammation. Front Pharmacol. 2023;14:1139654. https://doi.org/10.3389/fphar.2023.1139654
12. Alenazi F, Moursi S, Mahmoud MR, et al. Withaferin A alleviates inflammation in animal models of arthritis by inhibiting the NF-κB pathway and cytokine release. Chem Biol Interact. 2024;398:111114. https://doi.org/10.1016/j.cbi.2024.111114
13. Raut A, Tripathi R, Marathe PA, et al. Evaluation of Withania somnifera (L.) Dunal (Ashwagandha) on physical performance, biomarkers of inflammation, and muscle status in healthy volunteers: a randomized, double-blind, placebo-controlled study. Cureus. 2024;16(9):e68940. https://doi.org/10.7759/cureus.68940
14. Majeed M, Nagabhushanam K, Murali A, et al. A standardized Withania somnifera (Linn.) root extract with piperine alleviates the symptoms of anxiety and depression by increasing serotonin levels: a double-blind, randomized, placebo-controlled study. J Integr Complement Med. 2024;30(5):459–468.

https://doi.org/10.1089/jicm.2023.0279
15. Kim H, Choi HS, Han K, et al. Ashwagandha (Withania somnifera (L.) dunal) root extract containing withanolide a alleviates depression-like behavior in mice by enhancing the brain-derived neurotrophic factor pathway under unexpected chronic mild stress. J Ethnopharmacol. 2025;340:119224. https://doi.org/10.1016/j.jep.2024.119224
16. Rathi P, Kim SK. Randomized, double-blind, crossover study comparing the bioavailability of 4 Ashwagandha (Withania somnifera (L.) Dunal) extracts in healthy adults under fasting condition. Curr Ther Res Clin Exp. 2025;103:100805. https://doi.org/10.1016/j.curtheres.2025.100805
17. Ronen Y, Ebert C, Tamim-Yecheskel BC, et al. Comprehensive safety evaluation of Withania somnifera (Ashwagandha): an AI-driven meta-analysis and quantitative structure-activity relationship based toxicity assessment. Front Nutr. 2025;12:1658265. https://doi.org/10.3389/fnut.2025.1658265
18. Kashyap D, Roy R, Varshney N, et al. Withania somnifera extract reduces gastric cancerous properties through inhibition of gankyrin in cellular milieu produced by Helicobacter pylori and Epstein Barr virus. J Biomol Struct Dyn. 2024;42(18):9399–9415. https://doi.org/10.1080/07391102.2023.2252096
19. Fisch KM, Gamini R, Alvarez-Garcia O, et al. Identification of transcription factors responsible for dysregulated networks in human osteoarthritis cartilage by global gene expression analysis. Osteoarthritis Cartilage. 2018;26(11):1531–1538. https://doi.org/10.1016/j.joca.2018.07.012
20. Atasoy-Zeybek A, Hawse GP, Nagelli CV, et al. Transcriptomic changes during the replicative senescence of human articular chondrocytes. Int J Mol Sci. 2024;25(22):12130. https://doi.org/10.3390/ijms252212130
21. Clough E, Barrett T, Wilhite SE, et al. NCBI GEO: archive for gene expression and epigenomics data sets: 23-year update. Nucleic Acids Res. 2024;52(D1):D138–D144. https://doi.org/10.1093/nar/gkad965
22. Zdrazil B, Felix E, Hunter F, et al. The ChEMBL Database in 2023: a drug discovery platform spanning multiple bioactivity data types and time periods. Nucleic Acids Res. 2024;52(D1):D1180–D1192. https://doi.org/10.1093/nar/gkad1004
23. Kim S, Chen J, Cheng T, et al. PubChem 2023 update. Nucleic Acids Res. 2023;51(D1):D1373–D1380. https://doi.org/10.1093/nar/gkac956
24. Zerio CJ, Sivinski J, Wijeratne EMK, et al. Physachenolide C is a potent, selective BET inhibitor. J Med Chem. 2023;66(1):913–933. https://doi.org/10.1021/acs.jmedchem.2c01770
25. Robinson MD, McCarthy DJ, Smyth GK. edgeR: a Bioconductor package for differential expression analysis of digital gene expression data. Bioinformatics. 2010;26(1):139–140. https://doi.org/10.1093/bioinformatics/btp616
26. Chen Y, Chen L, Lun ATL, et al. edgeR v4: powerful differential analysis of sequencing data with expanded functionality and improved support for small counts and larger datasets. Nucleic Acids Res. 2025;53(2):gkaf018. https://doi.org/10.1093/nar/gkaf018
27. Ritchie ME, Phipson B, Wu D, et al. limma powers differential expression analyses for RNA-sequencing and microarray studies. Nucleic Acids Res. 2015;43(7):e47. https://doi.org/10.1093/nar/gkv007
28. Kolberg L, Raudvere U, Kuzmin I, et al. g:Profiler—interoperable web service for functional enrichment analysis and gene identifier mapping (2023 update). Nucleic Acids Res. 2023;51(W1):W207–W212. https://doi.org/10.1093/nar/gkad347
29. Szklarczyk D, Kirsch R, Koutrouli M, et al. The STRING database in 2023: protein–protein association networks and functional enrichment analyses for any sequenced genome of interest. Nucleic Acids Res. 2023;51(D1):D638–D646. https://doi.org/10.1093/nar/gkac1000
30. Milacic M, Beavers D, Conley P, et al. The Reactome Pathway Knowledgebase 2024. Nucleic Acids Res. 2024;52(D1):D672–D678. https://doi.org/10.1093/nar/gkad1025
31. Aleksander SA, Balhoff J, Carbon S, et al. The Gene Ontology knowledgebase in 2023. Genetics. 2023;224(1):iyad031. https://doi.org/10.1093/genetics/iyad031
32. Kanehisa M, Furumichi M, Sato Y, et al. KEGG for taxonomy-based analysis of pathways and genomes. Nucleic Acids Res. 2023;51(D1):D587–D592. https://doi.org/10.1093/nar/gkac963
33. Zhao Q, Xu T, Du Z, et al. Cartilage targeting hydrogel nanoplatform degrades BRD4 to alleviate osteoarthritis via Nav1.7 axis. Nat Commun. 2026;17(1):4573. https://doi.org/10.1038/s41467-026-71246-w

34. Sun J, Wang XH, Song FH, et al. Inhibition of Brd4 alleviates osteoarthritis pain via suppression of neuroinflammation and activation of Nrf2-mediated antioxidant signalling. Br J Pharmacol. 2023;180(24):3194–3214. https://doi.org/10.1111/bph.16195
35. Paradise CR, Galvan ML, Pichurin O, et al. Brd4 is required for chondrocyte differentiation and endochondral ossification. Bone. 2022;154:116234. https://doi.org/10.1016/j.bone.2021.116234
36. Negi V, Lee J, Mandi V, et al. Bromodomain protein inhibition protects β-cells from cytokine-induced death and dysfunction via antagonism of NF-κB pathway. Cells. 2024;13(13):1108. https://doi.org/10.3390/cells13131108
37. Gao X, Liu H, Guo J, et al. OGT regulates histone demethylation and alleviates osteoarthritis progression by O-GlcNAcylation of KDM6B. J Adv Res. 2026;87:455–471. https://doi.org/10.1016/j.jare.2026.01.003
38. Sylvestre M, Barbier N, Sibut V, et al. KDM6B drives epigenetic reprogramming associated with lymphoid stromal cell early commitment and immune properties. Sci Adv. 2023;9(48):eadh2708. https://doi.org/10.1126/sciadv.adh2708
39. Yang C, Dong W, Wang Y, et al. DDIT3 aggravates TMJOA cartilage degradation via Nrf2/HO-1/NLRP3-mediated autophagy. Osteoarthritis Cartilage. 2024;32(8):921–937. https://doi.org/10.1016/j.joca.2024.04.017
40. Hadzic E, To B, Pest MA, et al. Anabolic phenotype in cartilage-specific mitogen-inducible gene-6 knockout mice is independent of transforming growth factor-α. Osteoarthr Cartil Open. 2023;5(3):100387. https://doi.org/10.1016/j.ocarto.2023.100387
41. Zhang L, Shi Y, Yan M, et al. Modulatory action of withaferin-A on oxidative damage through regulation of inflammatory mediators and apoptosis via PI3K/AKT signaling pathway in high cholesterol-induced atherosclerosis in experimental rats. J Biochem Mol Toxicol. 2022;36(10):e23154. https://doi.org/10.1002/jbt.23154
42. Liu T, Wang J, Tong Y, et al. Integrating network pharmacology and animal experimental validation to investigate the action mechanism of oleanolic acid in obesity. J Transl Med. 2024;22(1):86. https://doi.org/10.1186/s12967-023-04840-x
43. Wang Z, Li R, Chen X, et al. Network pharmacology, molecular docking and experimental validation to elucidate the anti-T2DM mechanism of Lanxangia tsaoko. Fitoterapia. 2024;178:106117. https://doi.org/10.1016/j.fitote.2024.106117
44. Peng W, Yang Y, Lu H, et al. Network pharmacology combines machine learning, molecular simulation dynamics and experimental validation to explore the mechanism of acetylbinankadsurin A in the treatment of liver fibrosis. J Ethnopharmacol. 2024;323:117682. https://doi.org/10.1016/j.jep.2023.117682
45. Kim DU, Kweon B, Oh J, et al. A network pharmacology study and experimental validation to identify the potential mechanism of heparan sulfate on Alzheimer's disease-related neuroinflammation. Biomedicines. 2025;13(1):103. https://doi.org/10.3390/biomedicines13010103